N72-23794

STRATIFICATION CALCULATIONS IN A HEATED CYROGENIC OXYGEN STORAGE TANK AT ZERO GRAVITY

By John T. Suttles and G. Louis Smith

NASA Langley Research Center
Hampton, Virginia 23365

Abstract

A cylindrical one-dimensional model of the Apollo cyrogenic oxygen storage tank has been developed to study the effect of stratification in the tank. Zero gravity is assumed, and only the thermally induced motions are considered. The governing equations are derived from conservation laws and solved on a digital computer. Realistic thermodynamic and transport properties are used. Calculations were made for a wide range of conditions. The results show the fluid behavior to be dependent on the quantity in the tank or equivalently the bulk fluid temperature. For high quantities (low temperatures) the tank pressure rises rapidly with heat addition, the heater temperature remains low, and significant pressure drop potentials accrue (over 100 psia in 2 hours). For low quantities the tank pressure rises more slowly with heat addition and the heater temperature becomes high (as much as 500° K (440° F)). A high degree of stratification resulted for all conditions; however, the stratified region extended appreciably into the tank only for the lowest tank quantity. The calculations also indicate a significant flux of mass from the heater tube for high tank quantities. The results have been compared with Apollo 14 flight data. For attitude hold conditions (i.e. no spacecraft motions) the calculations are in good agreement with the data.

Introduction

The removal of the mixing fans from the supercritical oxygen storage tanks in the Apollo spacecraft introduces the possibility that the fluid in the tank can become stratified. Stratification, which results from the temperature gradients surrounding the heating element used for pressurization of the tank, can have several possibly serious effects. First it can cause erroneous quantity probe measurements with the potential for precipitating a mission abort. Second, if the low density fluid from the stratified layer enters the oxygen supply lines, the potential exists for fuel cell shutdown. Finally, if the stratified layer becomes too extensive, a perturbing force of even extremely low magnitude can cause depressurization with the potential for the existence of two phase fluid in the tank.

The purpose of this paper is to examine the extent of the stratification and the potential for depressurization which might exist in the supercritical oxygen storage tank. The worst case of no natural convection, has been assumed for the stratification calculations. The depressurization calculations are based on uniform (completely mixed) conditions in the tank. Zero gravity has been assumed throughout the analysis.

The approach which has been taken is to use a simple mathematical model which facilitiates a solution but retains the essential features of the actual cryogenic storage tank. For this purpose a one-dimensional cylindrical tank model is used. The governing equations are derived from the conservation laws and solved numerically on a digital computer. Realistic thermodynamic properties based on information from the National Bureau of Standards (ref. 1) and transport properties from ref. 2 are used throughout the analysis.

Symbols

A	area, m^2
C_p	specific heat, j/kg-^oK
k	thermal conductivity, j/m-sec-^oK
K	arbitrary constant
L	length, m
m	mass of fluid, kg
M	mass of heater tube, kg
$\vec{n}$	unit normal to tank surface
p	pressure, N/m^2 or psia
q	heat flux, watts/cm^2
Q	heat rate, watts
Q_{leak}	heat rate due to heat leak at tank wall, watts
Q_{input}	heat rate input to heater tube, watts
Q_{stored}	heat stored by heater tube, watts
Q_{net}	net heat rate to fluid (see equation 26), watts
r	radius of point in tank, m
t	time, sec.
T	temperature, ^oK or ^oF
v	radial velocity of fluid in tank, m/sec.
V	volume of tank, m^3
$\vec{V}$	velocity vector of fluid in tank, m/sec.
α	arbitrary function of time and space

∇	del operator
ϵ	emissivity
η	non-dimensional Lagrange space-coordinate
ϕ	function defined by equation (27)
ρ	fluid density, kg/m^3
σ	Stephan-Boltzmann constant, 5.6697×10^{-8} watts/$m^2\text{-}^oK^4$
θ	function defined by equation (28)

Subscripts

o	initial value
w	value at tank wall
HTR	value at heater
COND	result of conductivity
RAD	result of radiation
b	value at a boundary
$(\dot{})$	$\frac{d(\ )}{dt}$
$\frac{D(\ )}{Dt}$	substantive derivative of ( )
$\Delta(\ )$	increment in ( )

Analysis

Model and Basic Equations

A simplified tank model which includes the essential features of an actual storage tank is illustrated in figure 1. A cylindrical tank with a radius of .305 meters (1 foot) is assumed with variations in properties in the radial direction only (i.e., the model is one-dimensional). To provide a specified heat input for maintaining tank pressure a cylindrical heater tube with a radius of .025 meters (1 inch) is centered in the tank. A uniform heat leak is assumed to exist over the wall of the tank since cyrogenic storage tanks always experience such a heat leak. In order to retain the simplicity of the model the effect of fluid withdrawal is included by assuming a uniform mass flux through the tank wall.

For the model shown in figure 1 fluid exists inside the heater tube as it does in the actual tank. The heater tube in the actual tank is provided with numerous holes so that fluid may move in or out the tube. In the model two approaches were used to calculate the thermally induced flow in and out the heater tube. In one approach the tube was considered to be a separate tank. By assuming that the pressure in the tube is the same as that in the main tank, the mass flux from the heater tube can be calculated directly. In this approach no attempt was made to include the effect of the fluid leaving or entering the tube on the behavior of the fluid in the tank. In the other approach the tube and tank were considered to be one system. Since the heater tube mass flux can not be calculated directly in this method, the mass of fluid in the tube was computed at each time by integrating the fluid density over the volume of the tube. The mass flux for the tube was then calculated by differentiating the mass of fluid with time.

In this analysis a one-dimensional model of a supercritical cyrogenic oxygen storage tank in zero gravity is considered. For a zero gravity environment fluid velocities are generated only by thermal expansion and mass removal effects and thus are expected to be small. Therefore, viscous effects and inertial forces are neglected. An examination of the thermodynamic data for cyrogenic oxygen in reference 1 shows that for the pressure (700-900 psia) and temperatures (100-300°K) of interest the speed of sound varies from approximately 150 to approximately 900 meters per second. The speed of sound is therefore considerably larger than any expected fluid velocities. Thus pressure variations across the tank are negligible with respect to the mean pressure. The analysis is therefore based on the equations which follow:

continuity: $$\frac{D\rho}{Dt} + \rho\nabla\cdot\vec{V} = o \qquad (1)$$

momentum: $$\nabla p = o \qquad (2)$$

energy : $$\rho C_p \frac{DT}{Dt} = -\left(\frac{\partial\rho}{\partial T}\right)_p \frac{DP}{Dt} + \nabla\cdot(k\nabla T) - \nabla\cdot qRAD \qquad (3)$$

If pressure gradients are retained then the equations are hyperbolic and describe sound waves so that small characteristic times result. Neglecting the pressure gradients reduces the system to parabolic equations with considerably larger characteristic times and consequent savings in computer time.

To obtain a solution to the basic equations (1)-(3) an equation of state (i.e., $\rho = f(p,T)$), various thermodynamic properties $\left(C_p, \left(\frac{\partial\rho}{\partial T}\right)_p, \left(\frac{\partial\rho}{\partial p}\right)_T\right)$ and transport properties (k) are required. For this work the equation of state and required thermodynamic properties were obtained from the data in reference 1. The thermal conductivities were obtained from the data in reference 2. The data from the references has been arranged in the form of a table from which desired values are found using a table look-up scheme with first order interpolation.

The radiation transport term has been included in the energy equation since the work of reference 3 has indicated the possible importance of this mechanism. The absorption coefficient data used in that work however, is questionable. At the present time work is being done at the National Bureau of Standards, Boulder, Colorado to generate more meaningful data. When that data is available the effect of radiation energy transport can be evaluated with more confidence. The radiation effect has not been included in this analysis.

Stratified Tank Analysis

Development of equation. - As previously mentioned the tank characteristics of primary interest in this study are the tank pressure fluctuations and thermal stratification resulting from withdrawing fluid and cycling a heater to maintain the pressure in a specified range. The basic equations will therefore be utilized to develop an equation giving the tank pressure as a function of time and

an equation giving the temperatures in the tank as a function of space and time. With pressure and temperatures the density as a function of space and time can then be computed from the equation of state (data of ref. 1).

In the development of the pressure and temperature equations the use of the momentum equation is avoided by using a Lagrangian viewpoint for the substantive derivatives. That is, the substantive derivative is written as

$$\frac{D(\ )}{Dt} = \left[\frac{\partial(\ )}{\partial t}\right]_{particle} \tag{4}$$

so that particles (small volume elements) are followed in the solution. In the one-dimensional analysis being used the particles or small volume elements can be followed by using the condition that the particle mass is constant. Thus

$$\rho_o dV_o = \rho dV$$

where the subscript "o" denotes values at the initial time and the unsubscripted quantities are values at a subsequent time. For one-dimensional cylindrical coordinates

$$\rho_o r_o dr_o = \rho r dr \tag{5}$$

where r_o and r represent the initial and subsequent position of a particle. The simplicity of using the Lagrangian viewpoint is obtained by transforming to the initial (r_o) coordinates for the computation and transforming back to the actual coordinates (r) to analyse the results.

One possible complication does arise with the use of the Lagrangian viewpoint because with mass removal occurring particles are leaving the system. At each time the initial coordinate of the particle at the tank wall must be determined and particles with larger initial coordinates must be considered to have left the system. To avoid the problem resulting from this continuous change in the coordinate system, a set of non-dimensional initial coordinates can be defined. The non-

dimensional coordinates are given by

$$\eta = \frac{r_o}{r_{o,w}} \tag{6}$$

where $r_{o,w}$ is a function of time and can be obtained by considering the loss of mass from the system in time dt

$$\dot{r}_{o,w} = \frac{dr_{o,w}}{dt} = \frac{\dot{m}}{2\pi L \rho_w r_{o,w}} \tag{7}$$

$$r_{o,w} = \int_o^t \dot{r}_{o,w} dt \tag{8}$$

To transform partial differential equations from r_o,t coordinates to η,t coordinates the required relations are

$$\left[\frac{\partial(\ )}{\partial r_o}\right]_t = \frac{1}{r_{o,w}}\left[\frac{\partial(\ )}{\partial \eta}\right]_t \tag{9}$$

$$\left[\frac{\partial(\ )}{\partial t}\right]_{r_o} = \left[\frac{\partial(\ )}{\partial t}\right]_\eta - \eta \frac{\dot{r}_{o,w}}{r_{o,w}} \frac{\partial(\ )}{\partial \eta} \tag{10}$$

The pressure equation development is begun by dividing the continuity equation (equation 1) by ρ and integrating over the tank volume

$$\int_V \frac{1}{\rho} \frac{D\rho}{Dt} dV + \int_V \nabla \cdot \vec{V} dV = o \tag{11}$$

The Gauss Theorem can be applied to the second integral to obtain

$$\int_V \frac{1}{\rho}\frac{D\rho}{Dt}\,dV + \int_A \vec{V}\cdot\vec{n}\,dA = o$$

Since uniform mass flux over the tank surface has been assumed then

$$\int_A \vec{V}\cdot\vec{n}dA = v_w A_w = -\frac{\dot{m}}{\rho_w}$$

where the convention is taken that a positive velocity will produce a negative mass flux. Thus,

$$\int_V \frac{1}{\rho}\frac{D\rho}{Dt}\,dV = \frac{\dot{m}}{\rho_w} \tag{12}$$

If the density is considered to be a function of pressure and temperature then

$$\frac{D\rho}{Dt} = \left(\frac{\partial\rho}{\partial P}\right)_T \frac{Dp}{Dt} + \left(\frac{\partial\rho}{\partial T}\right)_p \frac{DT}{Dt}$$

and since $\nabla p = o$ then $\frac{Dp}{Dt} = \frac{\partial p}{\partial t}$ which is uniform in the volume. Using these conditions in equation (12) it follows that

$$\frac{\partial p}{\partial t} = \frac{\frac{\dot{m}}{\rho_w} - \int_V \frac{1}{\rho}\left(\frac{\partial\rho}{\partial T}\right)_p \frac{DT}{Dt}\,dV}{\int_V \frac{1}{\rho}\left(\frac{\partial\rho}{\partial p}\right)_T dV} \tag{13}$$

is the equation governing the pressure changes. Equation (13) and the energy equation (equation (3) without the radiation term) both contain $\frac{\partial p}{\partial t}$ and $\frac{DT}{Dt}$ so they are solved simultaneously to give

$$\frac{\partial p}{\partial t} = \frac{\frac{\dot{m}}{\rho_w} - \int_V \left\{ \frac{1}{\rho^2 C_p} \left(\frac{\partial \rho}{\partial T}\right)_p \nabla\cdot(k\nabla T) \right\} dV}{\int_V \frac{1}{\rho}\left\{ \left(\frac{\partial \rho}{\partial p}\right)_T - \frac{T}{\rho^2 C_p}\left[\left(\frac{\partial \rho}{\partial T}\right)_p\right]^2 \right\} dV} \tag{14}$$

and

$$\frac{DT}{Dt} = -\left(\frac{\partial \rho}{\partial T}\right)_p \frac{T}{\rho^2 C_p}\left(\frac{\partial p}{\partial t}\right) + \frac{1}{\rho C_p} \nabla\cdot(k\nabla T) \tag{15}$$

where equation (14) can be used first to obtain $\frac{\partial p}{\partial t}$ which appears in equation (15).

For one-dimensional cylindrical coordinates

$$dV = 2\pi L r dr$$

where L is an arbitrary length chosen to produce a desired tank volume and

$$\nabla\cdot(k\nabla T) = \frac{1}{r}\frac{\partial}{\partial r}\left(kr\frac{\partial T}{\partial r}\right)$$

Since it is desired to work in the Lagrangian viewpoint the transformations defined by equations (5-10) are used so that equations (14) and (15) become

$$\frac{\partial p}{\partial t} = \frac{\frac{\dot{m}}{2\pi L \rho_w} - \int_{\eta_1}^{1} \frac{1}{r_{o,w}\rho_o \rho^2 C_p}\left(\frac{\partial \rho}{\partial T}\right)_p \frac{\partial}{\partial \eta}\left(k \frac{r^2}{r_{o,w} r_o}\rho \frac{\partial T}{\partial \eta}\right) d\eta}{\int_{\eta_1}^{1} \frac{\rho_o r_o r_{o,w}}{\rho^2}\left\{\left(\frac{\partial \rho}{\partial p}\right)_T - \frac{T}{\rho^2 C_p}\left[\left(\frac{\partial \rho}{\partial T}\right)_p\right]^2\right\} d\eta} \tag{16}$$

$$\left(\frac{\partial T}{\partial t}\right)_{particle} = -\left(\frac{\partial \rho}{\partial T}\right)_p \frac{T}{\rho^2 C_p} \frac{\partial p}{\partial t} + \frac{1}{\rho_o^2 C_p r_o r_{o,w}} \frac{\partial}{\partial \eta}\left(\frac{k r^2 \rho}{r_{o,w} r_o} \frac{\partial T}{\partial \eta}\right) - \eta \frac{\dot{r}_{o,w}}{r_{o,w}} \frac{\partial T}{\partial \eta} \tag{17}$$

where $\eta, r_{o,w}$ and $\dot{r}_{o,w}$ are defined by equations (6), (7), and (8) respectively. To find the location of particles equation (5) is used to obtain

$$\left[\frac{r^2}{2}\right]_{r_1}^{r} = \int_{r_{o,1}}^{r_o} \frac{\rho_o}{\rho} r_o dr_o \tag{18}$$

Boundary conditions.- Since equation (17) is a second order partial differential equation, two boundary conditions are required. For the fluid in the heater tube a symmetry condition is applied at the center of the tube

$$\left(\frac{\partial T}{\partial r}\right)_{r=o} = 0 \tag{19}$$

and the temperature of the fluid at the heater tube wall is equated with the heater temperature.

$$T = T_{HTR} \tag{20}$$

For the fluid outside the heater tube, the temperature of the fluid at the heater tube wall is equated to the heater temperature

$$T = T_{HTR} \tag{21}$$

and at the tank wall a heat flux (heat leak is imposed)

$$Q_{leak} = -\left(k \frac{\partial T}{\partial r}\right)_w A_w \tag{22}$$

For two of the boundary conditions the heater temperature is required. To determine its temperature the heater tube is considered to be a lumped mass and a heat balance is computed. The elements shown on figure 1, are considered to obtain

$$Q_{stored} = Q_{input} - \Sigma\, Q_{COND} - \Sigma\, Q_{RAD}$$

$$M_{HTR}C_{p,HTR}\frac{\partial T_{HTR}}{\partial t} = Q_{INPUT} - \left[\left(k\frac{\partial T}{\partial r}\right)_{\substack{\text{inside}\\ \text{HTR WALL}}} - \left(k\frac{\partial T}{\partial r}\right)_{\substack{\text{outside}\\ \text{HTR WALL}}}\right]\times$$

$$A_{HTR} - \varepsilon_{HTR}\,\sigma\left(T_{HTR}^4 - T_w^4\right)A_{HTR} \qquad (23)$$

which is the equation used to find the heater temperature.

Uniform Tank Analysis

For a uniform tank the temperature and density are constant over the tank volume. Equations (14) and (15) can be simplified for this case by performing the volume integrals in equation (14) and by integrating equation (15) over the tank volume. The results are

$$\frac{\partial p}{\partial t} = \frac{\dot{m} - \frac{1}{\rho C_p}\left(\frac{\partial \rho}{\partial T}\right)_p Q_{net}}{\left\{\left(\frac{\partial \rho}{\partial p}\right)_T - \frac{T}{\rho^2 C_p}\left[\left(\frac{\partial \rho}{\partial T}\right)_p\right]^2\right\}V} \qquad (24)$$

and

$$\frac{\partial T}{\partial t} = -\left(\frac{\partial \rho}{\partial T}\right)_p \frac{T}{\rho^2 C_p}\frac{\partial p}{\partial t} + \frac{1}{\rho C_p}\frac{Q_{net}}{V} \qquad (25)$$

where the Gauss Theorem has been used to write

$$\int_V \nabla\cdot(k\nabla T)\,dV = \int_A (k\nabla T)\cdot\vec{n}\,dA \qquad (26)$$

$$= \Sigma\, Q_{COND} + \Sigma\, Q_{RAD} = Q_{net}$$

If one defines

$$\phi = \frac{1}{\left\{\left(\frac{\partial \rho}{\partial p}\right)_T - \frac{T}{\rho^2 C_p}\left[\left(\frac{\partial \rho}{\partial T}\right)_p\right]^2\right\}} \tag{27}$$

and

$$\theta = -\frac{1}{\rho C_p}\left(\frac{\partial \rho}{\partial T}\right)_p \tag{28}$$

then (25) and (26) can be written in the simpler form

$$\frac{\partial p}{\partial t} = \frac{\phi}{V}\dot{m} + \frac{\phi\theta}{V} Q_{net} \tag{29}$$

$$\frac{\partial T}{\partial t} = \frac{\theta T}{\rho}\frac{\partial p}{\partial t} + \frac{Q_{net}}{\rho C_p V} \tag{30}$$

Numerical Method

The stratified tank calculations are performed by solving the partial differential equations given by (16) and (17) with boundary conditions given by equations (19) - (23). Equations (6) - (8) and (18) are used to convert the normalized Lagrangian space coordinate η to the physical coordinates r. For the uniform tank calculations the ordinary differential equations given by (29) and (30) are solved. The numerical method employed is to replace the derivaties in each equation by appropriate finite difference approximations and advance the solution in time. The integrals in equation (16) are evaluated using the trapezoidal rule.

Finite difference expressions. - For purposes of illustration an arbitrary function of time and space $\alpha(t,r)$ is considered. The difference expressions are:

$$\frac{\partial \alpha}{\partial t} = \frac{\alpha(t + \Delta t, r) - \alpha(t,r)}{\Delta t} \tag{31}$$

$$\frac{\partial \alpha}{\partial r} = \frac{\alpha(t,r + \Delta r) - \alpha(t,r - \Delta r)}{2\Delta r} \tag{32}$$

$$\frac{\partial^2 \alpha}{\partial r^2} = \frac{\alpha(t,r + \Delta r) - 2\alpha(t,r) + \alpha(t,r - \Delta r)}{\Delta r^2} \tag{33}$$

For functions of time only an expression like equation (31) is used. At the boundary points the difference expression used for $\frac{\partial \alpha}{\partial r}$ is

$$\left(\frac{\partial \alpha}{\partial r}\right)_b = \frac{\alpha(t,r_b) - \alpha(t,r_b \pm \Delta r)}{\mp \Delta r} \tag{34}$$

where the signs (±) are selected depending on whether the boundary is a right hand or left hand boundary.

If a boundary condition of the form

$$\left(\frac{\partial \alpha}{\partial r}\right)_b = K \tag{35}$$

is specified then $\left(\frac{\partial^2 \alpha}{\partial r^2}\right)_b$ is written as

$$\left(\frac{\partial^2 \alpha}{\partial r^2}\right)_b = \frac{K - \left[\frac{\alpha(t,r_b) - \alpha(t,r_b \pm \Delta r)}{\mp \Delta r}\right]}{\Delta r} \tag{36}$$

Stability. - In a finite difference approach such as that used the stability of the computing scheme must be considered. The equations of interest as far as stability is concerned are equations (16) and (17). A linear stability analysis applied to equation (17) yields

$$\Delta t < \frac{1}{\left[\frac{2kr^2\rho}{r_o^2 \rho_o^2 C_p (\Delta r)^2} + \frac{1}{\rho^2 C_p}\left(\frac{\partial \rho}{\partial T}\right)_p \frac{\partial p}{\partial t}\right]} \tag{37}$$

as a restriction on the time step size. However, the integral nature of equation (16) precludes any simple stability analysis of that equation. Therefore it was decided to use equation (37) to define the time steps for both equations. Because of the uncertainty with regard to the stability of equation (16) the results must be checked by making calculations for a range of time step sizes and noting the changes in the solutions. The results of such a procedure are discussed in the section which follows:

Results and Discussion

Calculated Results

Calculations for a uniform tank have been made and the results are presented in figure 2. The calculations give the time rate of change of pressure as a function of temperature for a range of mass flux rates both for heat addition (Q_{net} = 125 watts) and for no heat addition. The results indicate that for temperatures up to near critical values (i.e., near critical temperatures are between 155 and 165°K) the magnitude of the pressure derivative is relatively high and varies significantly with temperature whereas at higher temperatures the magnitude is relatively low and the variations are only slight. The unusual variations in the pressure derivative in the near-critical region reflects the rapid changes in thermodynamic properties in this region. These results also show that the mass flux rate has a strong influence at temperatures below the near critical region but has only a weak influence at higher temperatures.

Stratified tank calculations for four typical tank operating conditions have been made. The tank and heater physical properties which were used for all the computations are given in Table I. Input values for each of the four cases computed are given in Table II. Because of the questionable stability of equation (16) each of the cases was calculated with the time step size determined by 1/3 of the expression in equation (37) and for values successively smaller until the solution became stationary with respect to step size changes. The time step sizes determined for stability of cases 1 and 2 were about an order of magnitude lower than the initially computed values whereas the initially computed values were found to be adequate for cases 3 and 4. The results for cases 1-4 are presented in figures 3-14. The quantities shown are the time histories of heater temperature, tank pressure, and heater tube mass flux and profiles of temperature and density across the tank for pertinent simulated times. The pressure change potentials are indicated in the results by the differences between the stratified tank pressure and

the associated uniform tank pressure. The degree and extent of stratification in the tank is assessed by examining the temperature and density profiles.

The time histories in figure 3 show that cases 1 and 2 have the same characteristic feature, that is many heater cycles occurred during the two-hour simulated time of the calculations. In contrast less than one heater cycle was obtained for cases 3 and 4. This difference in characteristic behavior is probably due to the fact that the initial temperatures of cases 1 and 2 are in the sensitive range below the near critical region whereas the initial temperature of case 3 is in the near critical region and that for case 4 is considerably higher. It should be noted that the relative insensitivity of the tank pressure to heat input for the lowest density cases (cases 3 and 4) causes the heater temperature to reach quite high values ($T_{HTR} > 500^{o}K$ for case 4). The very high frequency heater cycling for case 1 apparently results when the heater temperature becomes stationary ("locked" or "trapped") in the near critical temperature region. In this regard it is noted that when the heater temperature for case 2 is in the near critical region the heater cycles at a relatively high rate but the rate diminishes as the heater temperature rises above the near critical region.

Results for the possibility of a pressure change caused by mixing indicate significant pressure drop potentials for cases 1 and 2 (100 and 120 psia respectively at t = 120 min), initially a pressure drop potential and later a pressure rise potential for case 3, and significant pressure rise potentials for case 4 (60 psia at t = 120 min). These pressure rise potentials are in disagreement with analyses of other investigators (see for example reference 4) and require further study.

The heater mass flux rates obtained are presented in figure 4. The results presented are for the separate heater tube and tank model only. These results show that the heater mass flux rates for cases 1 and 2 are relatively high compared to the mass flux rate of the tank whereas the rates for cases 3 and 4 are relatively low. The calculations indicate that fluid leaves the heater tube when the heater is on and enters the tube when the heater is off. Thus for some tank operating conditions this mechanism may be important as far as inducing convective motions of the fluid.

Heater mass flux rate results considering the tank as one system are not available because of excessive computer time required. In this approach the heater location moves from node to node because of the Lagrangian coordinate system used. As a consequence a fine nodal spacing and hence very large computational times were required to

avoid numerical difficulties. However, a limited number of calculations using this approach have been made. They indicate that the heater tube mass fluxes may be as much as a factor of 2 lower than those calculated by the separate heater tube approach. The gross tank behavior however is not significantly effected.

Profiles of temperature and density in the tank are presented in figure 5 for simulated times which were judged to be pertinent as far as illustrating the stratifications obtained. It is seen that the degree of stratification is significant in all the cases. For example, the density in the area next to the heater is 1/2 to 1/4 of the density in the outer portion of the tank. However, except for case 4, the extent of the stratification is confined to a region very close (within about .025 m (1 in.)) to the heater. For case 4 the density (and temperature) stratification is significant and extends far into the tank. For cases 3 and 4 the increase in density in the unstratified portion of the tank over the initial value is a result of the work done on that portion of the fluid by the expansion of the stratified fluid near the heater.

Comparison With Flight Data.

The calculations just described have been compared with Apollo 14 flight data. The comparisons are of the heater temperature and tank pressure and are presented in figures 6-9. Cases 1 and 2 are high quantity cases (95% and 75% respectively) for times when the spacecraft is in an attitude hold condition. Cases 3 and 4 are moderate to low quantity cases (52% and 12% respectively) for times when the spacecraft is spinning for passive thermal control (PTC). Since the calculation method presented here considers only thermally induced motions, then it should be expected that a better agreement between calculated and flight data would be obtained for cases 1 and 2 than for cases 3 and 4. An examination of figures 6-9 shows this to be true.

For cases 1 and 2 the calculations correctly predict the general characteristics of the heater cycling and the maximum heater temperature. The flight data in figure 6 show the existance of the condition previously discussed in the calculated data where the heater temperature becomes nearly stationary in the near-critical region and the heater begins cycling at a high frequency. The comparison in figure 7 indicates that for early simulation times the calculations do not agree well with the flight data. For latter simulation times when stratifications have accrued the calculations agree well with the data.

For cases 3 and 4 the calculations are seen to over predict both the time for the heater cycle and the maximum heater temperature.

In figure 8 note that after the heater is shut-off the pressure does not decay as rapidly in the calculations as in the data. Also the heater temperature is higher in the calculation than in the data for the entire heater cycle. These differences are attributed to the fact that the present calculation method neglects the convective transport mechanisms resulting from the spacecraft motions. The differences in the pressure cycle in figure 9 are not adequately understood. However the differences in the heater temperature again indicate an effect due to convective energy transport.

Conclusions

Calculations have been made of the behavior of supercritical oxygen in a storage tank in zero gravity while fluid is withdrawn and a heater is cycled to maintain the tank pressure in the range of 5.9295×10^6 N/m^2 (860 psia) to 6.2116×10^6 N/m^2 (900 psia). A one-dimensional model was used and the thermally induced movemoment of the fluid was the only motion considered. Four cases representing a wide range of tank operating conditions were considered. Based on the results obtained the following general conclusions are made:

1. For initial temperatures below near-critical, the tank pressure oscillates at a relatively high rate and the heater temperature remains low whereas for initial temperatures above near critical the tank pressure changes slowly and high heater temperatures result.

2. The results for pressure change potentials have indicated that for initial temperatures below near-critical,significant pressure drop potentials accrue (over 100 psia in 2 hours).

3. For initial conditions below the near-critical values the flux of fluid mass into and out of the heater tube is significant and may be important as far as inducing convective motion of the fluid.

4. A high degree of stratification was obtained for all cases considered however the stratified region extended appreciably into the tank only for the case with highest initial temperature, 194^{o}K.

5. A comparison of the calculations with Apollo 14 flight data has indicated that for attitude hold conditions the calculations are in good agreement with the flight data but for conditions when the spacecraft is spinning the calculations over predict the heater temperature and the time for a heater cycle.

References

1. Weber, L. A.: "Thermodynamic and Related Properties of Oxygen from the Triple Point to 300 K at Pressures to 330 Atmospheres," NBS Report 9710, June 20, 1968.

2. Stiel, L. I., and Thodos, George: "The Prediction of the Transport Properties of Pure Gaseous and Liquid Substances," Progress in International Research on Thermodynamic and Transport Properties. ASME, New York, 1962, p. 352.

3. Sollami, B. J., and Abraham, W. H.: "Heat-Transfer Characteristics of a Supercritical Cryogenic Storage System in Space," Bendix Technical Journal, Vol. 3, Spring 1970, p. 34-40.

4. Kamat, D. V., and Abraham, W. H.: "Pressure Collapse in Oxygen Storage Under Zero-g," Journal of Spacecraft and Rockets, Vol. 5, No. 2, Feb. 1968, pp. 184-188.

TABLE I

Physical Properties Used in Calculations

Tank Radius = 0.305 m (1.0 ft)

Tank Length = 0.463 m (1.52 ft)

Tank Volume = 0.135 m^3 (4.75 ft^3)

Heater on Pressure = 5.9295 x 10^6 N/m^2 (860 psia)

Heater off Pressure = 6.2116 x 10^6 N/m^2 (900 psia)

Heater Radius = 0.025 m (1. in.)

Heater Mass = 1.13 kg (2.5 lbm)

Heater Specific Heat = 460. j/kg-°K (0.11 Btu/lbm-°F)

Heater Emissivity = 0.3

Computing Nodes inside Heater Tube = 6

Computing Nodes in Main Tank = 57

TABLE II

Input Conditions for Stratified Tank Calculations

Case 1 - Attitude hold, approximately 95% quantity

T_o = 110°K (198°R)

P_o = 5.9295×10^6 N/m^2 (860 psia)

ρ_o = 1054.5 kg/m^3 (65.83 lbm/ft^3)

Q_{input} = 123.03 watts (419.82 Btu/hr)

Q_{leak} = 8.06 watts (27.5 Btu/hr)

$\dot{m}$ = -0.00011 kg/sec (0.87 lb/hr)

Case 2 - Attitude hold, approximately 75% quantity

T_o = 142°K (255°R)

P_o = 5.9295×10^6 N/m^2 (860 psia)

ρ_o = 837.76 kg/m^3 (52.30 lbm/ft^3)

Q_{input} = 123.24 watts (420.53 Btu/hr)

Q_{leak} = 6.45 watts (22.0 Btu/hr)

$\dot{m}$ = -0.000116 kg/sec (0.92 lb/hr)

TABLE II (concluded)

Case 3 - Passive thermal control (PTC)-approximately 52% quantity

T_o = 157°K (283°R)

P_o = 5.925×10^6 N/m^2 (860 psia)

ρ_o = 536.4 kg/m^3 (33.49 lbm/ft^3)

Q_{input} = 111.45 watts (380.30 Btu/hr)

Q_{leak} = 4.55 watts (15.5 Btu/hr)

$\dot{m}$ = -.000155 kg/sec (1.23 lb/hr)

Case 4 - Passive thermal control, approximately 12% quantity

T_o = 194°K (350°R)

P_o = 5.9295×10^6 N/m^2 (860 psia)

ρ_o = 148.73 kg/m^3 (9.28 lbm/ft^3)

Q_{input} = 111.45 watts (380.30 Btu/hr)

Q_{leak} = 4.25 watts (14.5 Btu/hr)

$\dot{m}$ = -.000107 kg/sec (0.85 lb/hr)

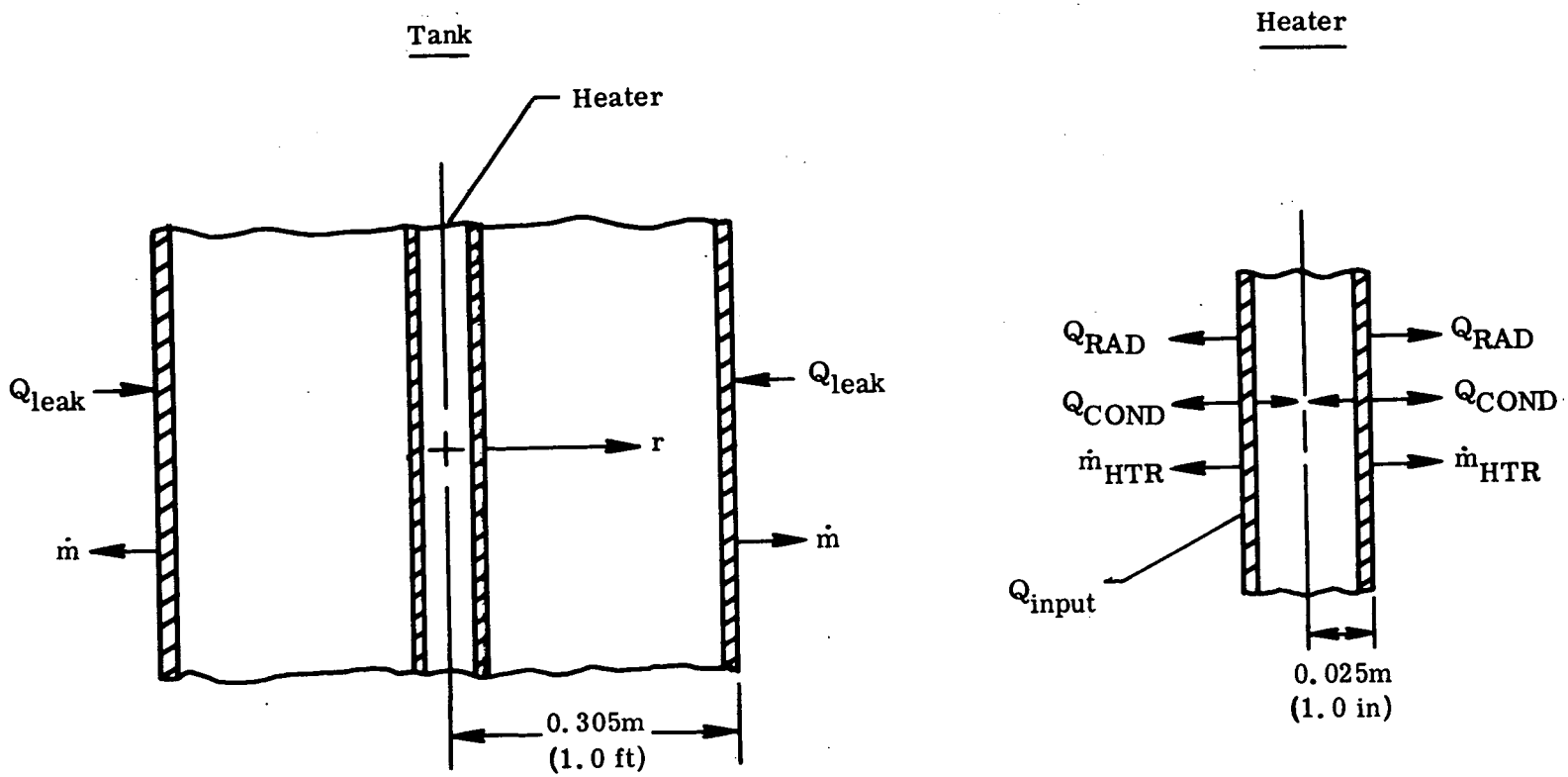

Figure 1. - Sketch of tank and heater showing essential features of model.

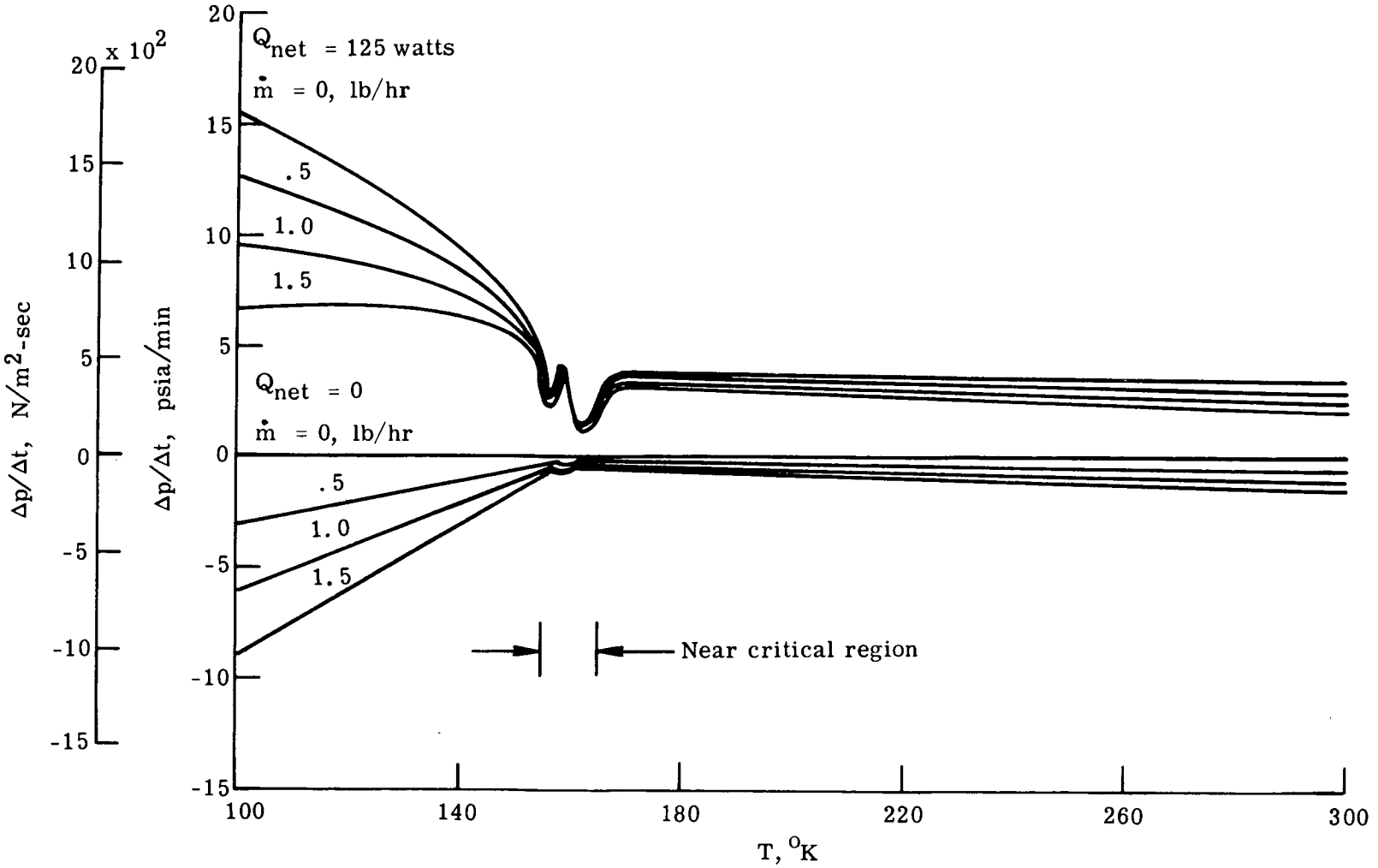

Figure 2. - Time rate of change of pressure in a uniform tank. p = 5.9295 x 10^6 N/m^2 (860 psia), V = 0.135 m^3 (4.75 ft^3).

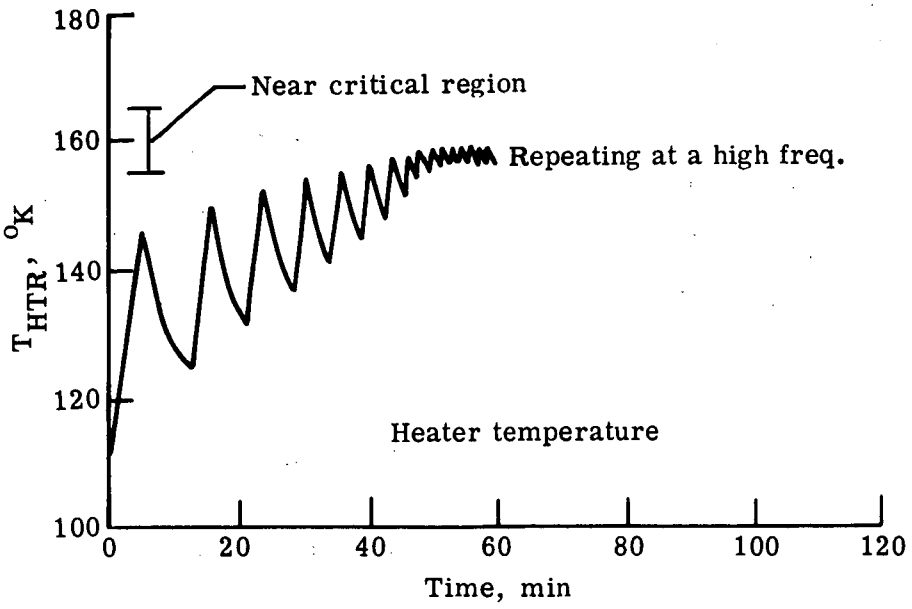

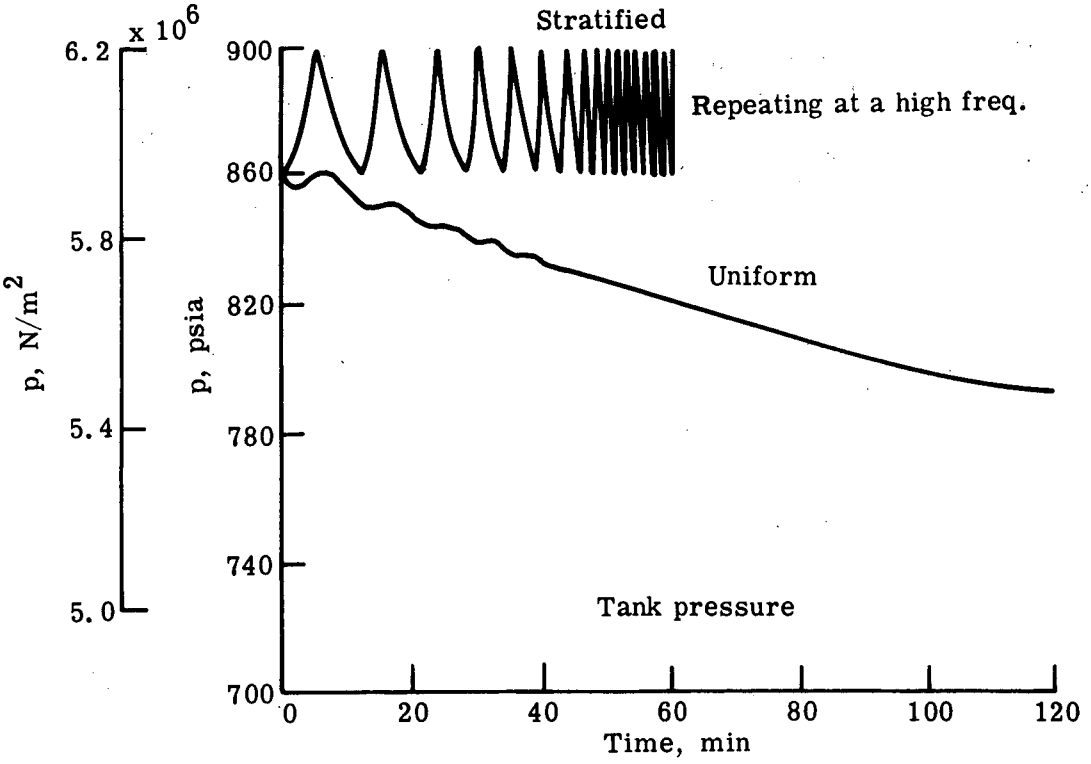

(a) Case 1.

Figure 3. - Time histories of heater temperature and tank pressure for cases 1-4.

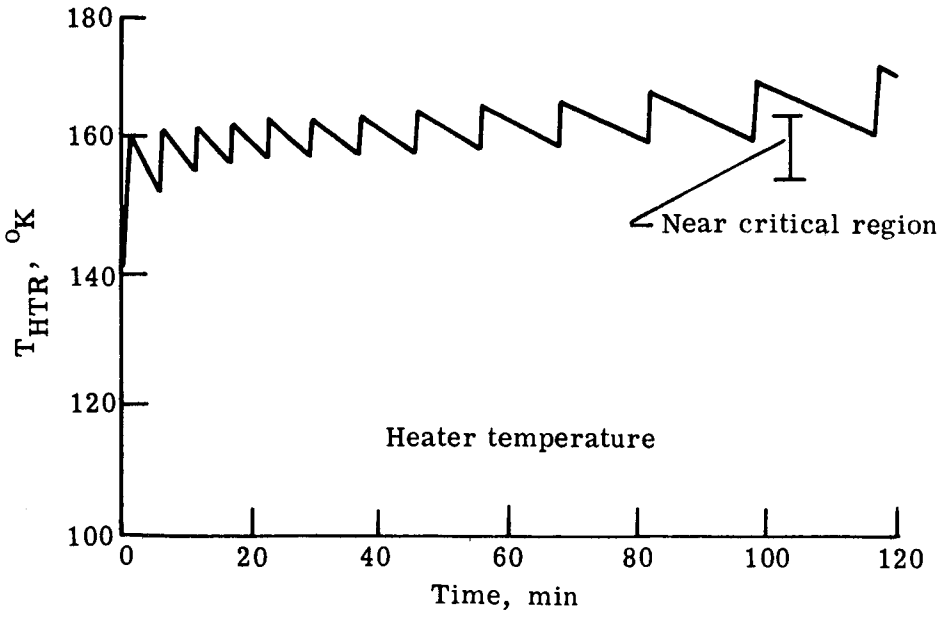

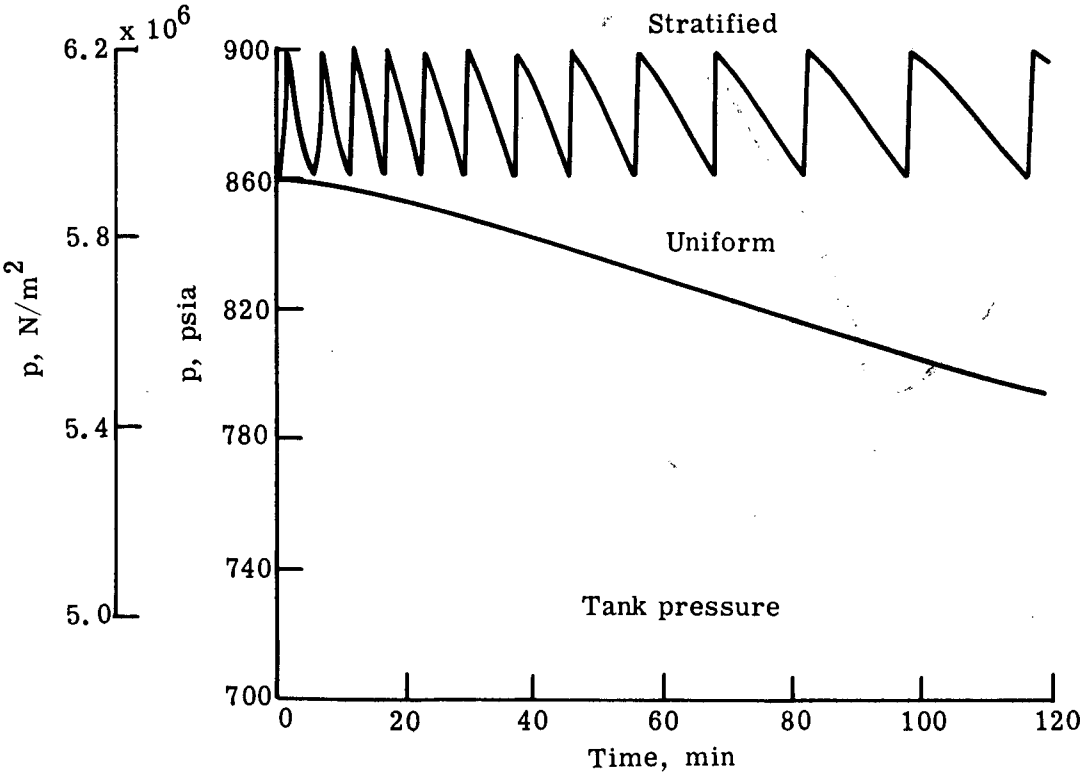

(b) Case 2.

Figure 3. - Continued.

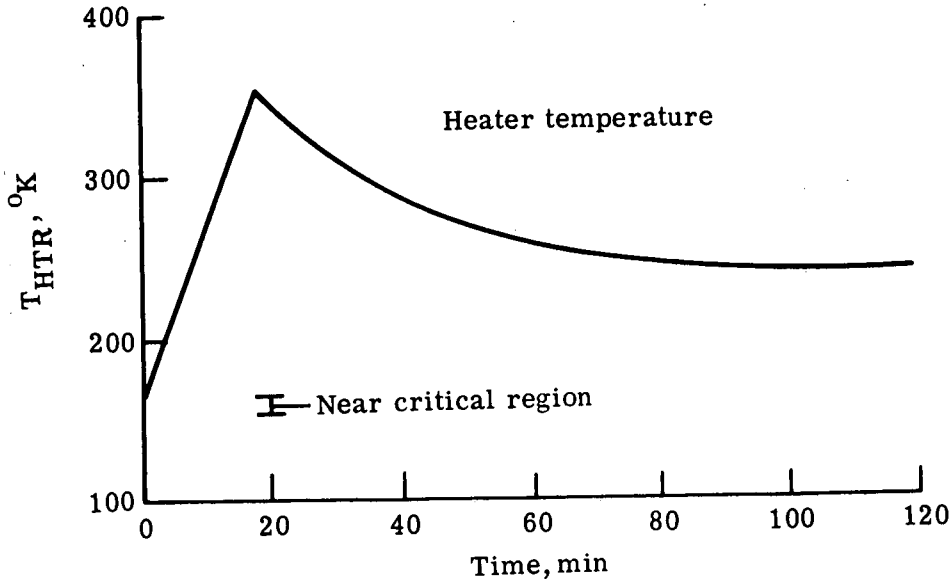

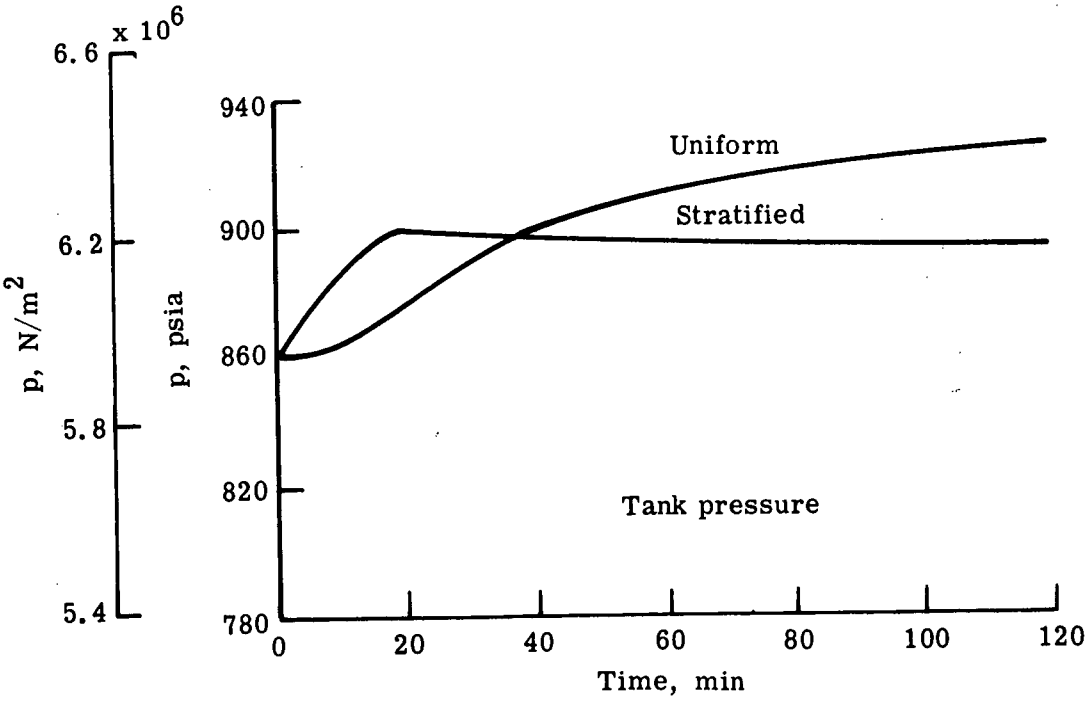

(c) Case 3.

Figure 3. - Continued.

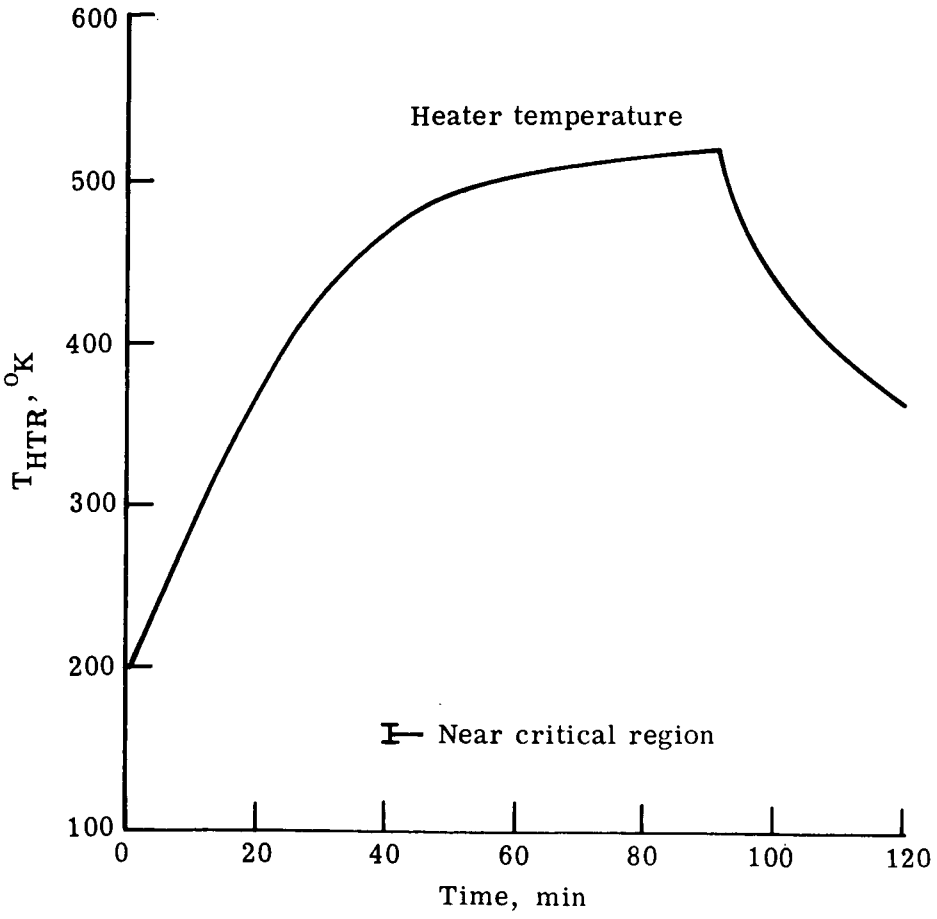

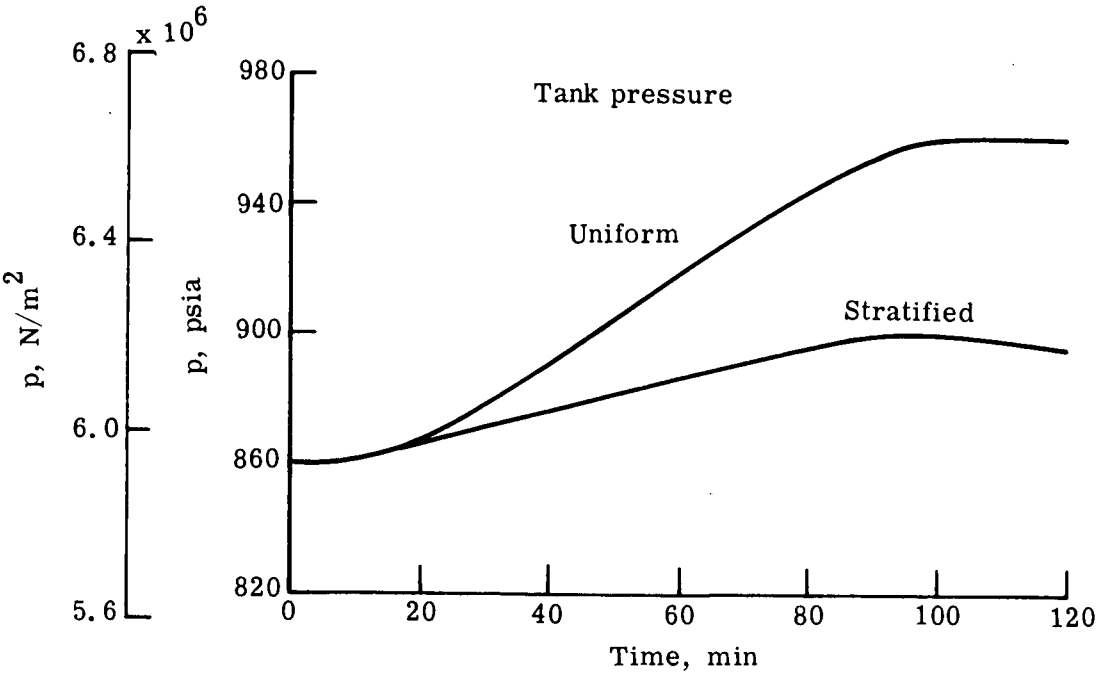

(d) Case 4.

Figure 3. - Concluded.

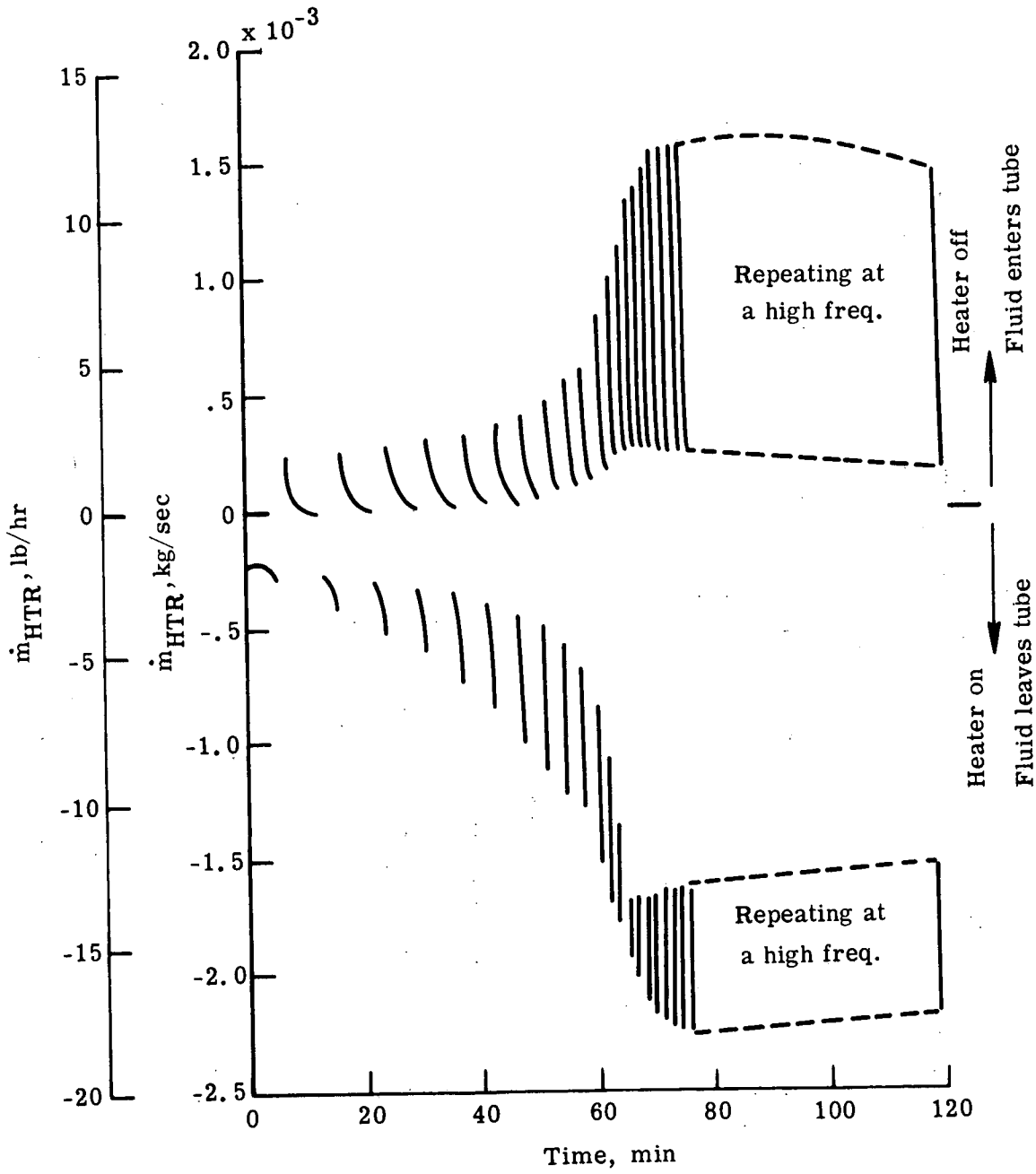

(a) Case 1.

Figure 4. - Time history of heater mass flux.

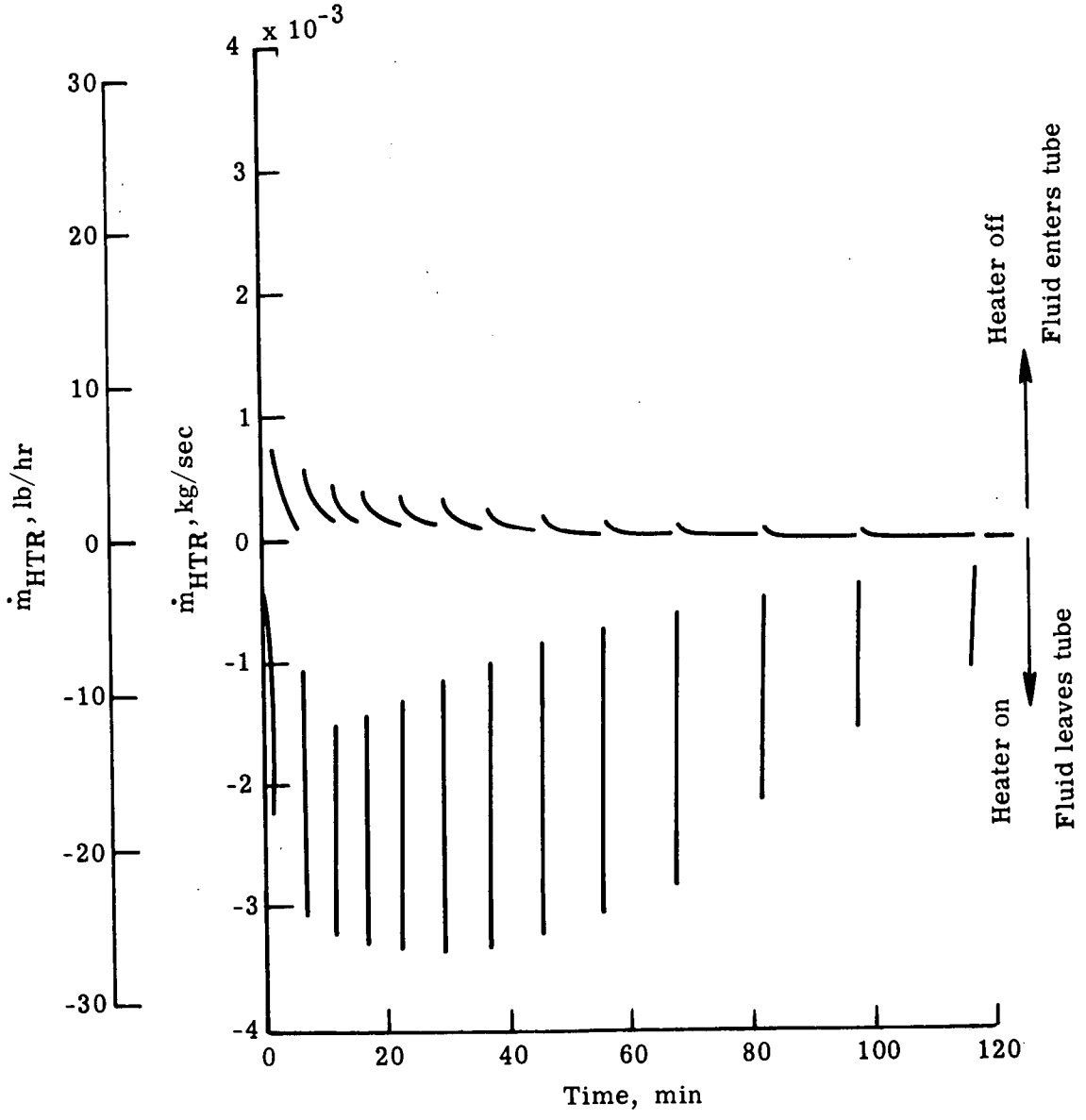

(b) Case 2.

Figure 4. - Continued.

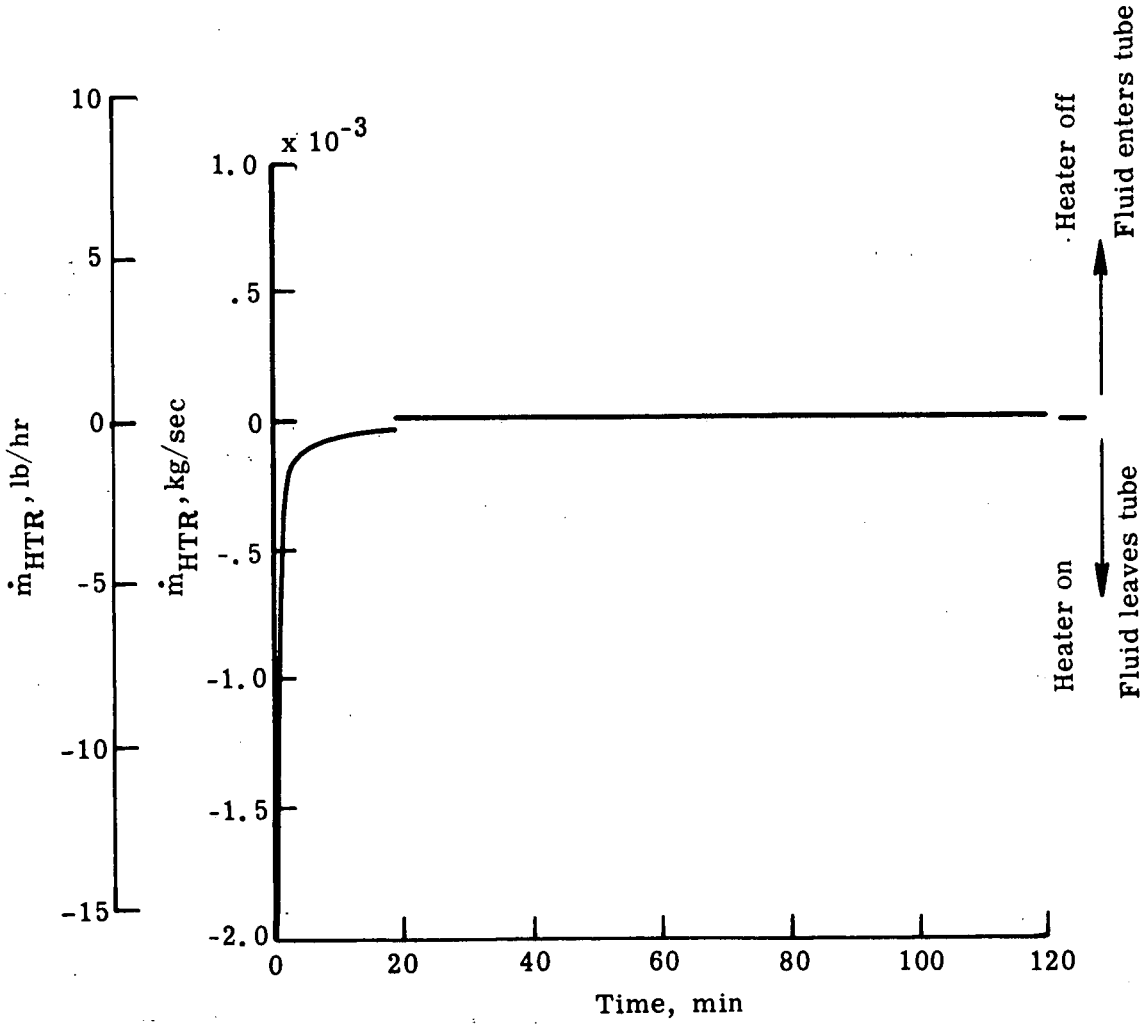

(c) Case 3.

Figure 4. - Continued.

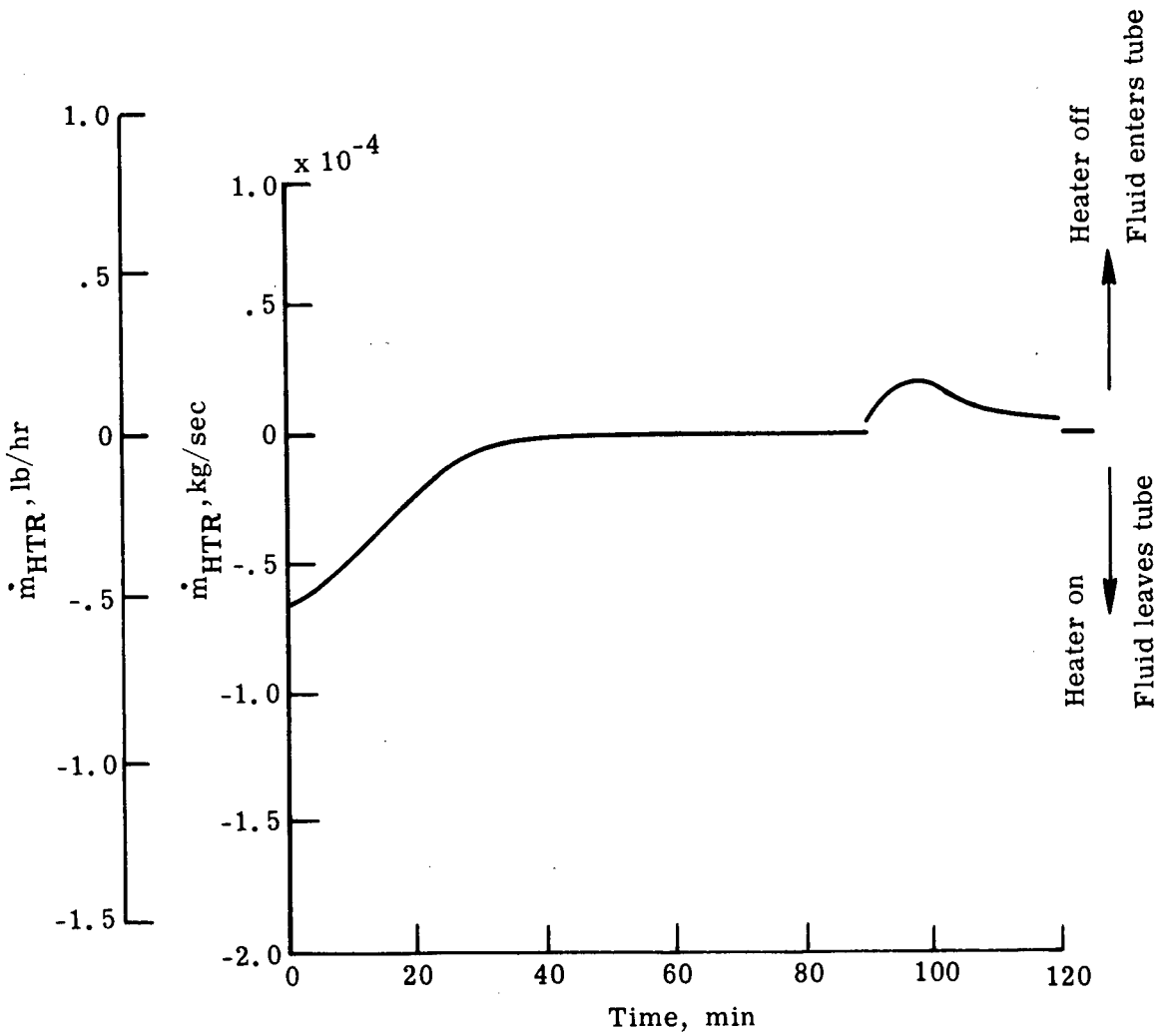

(d) Case 4.

Figure 4. - Concluded.

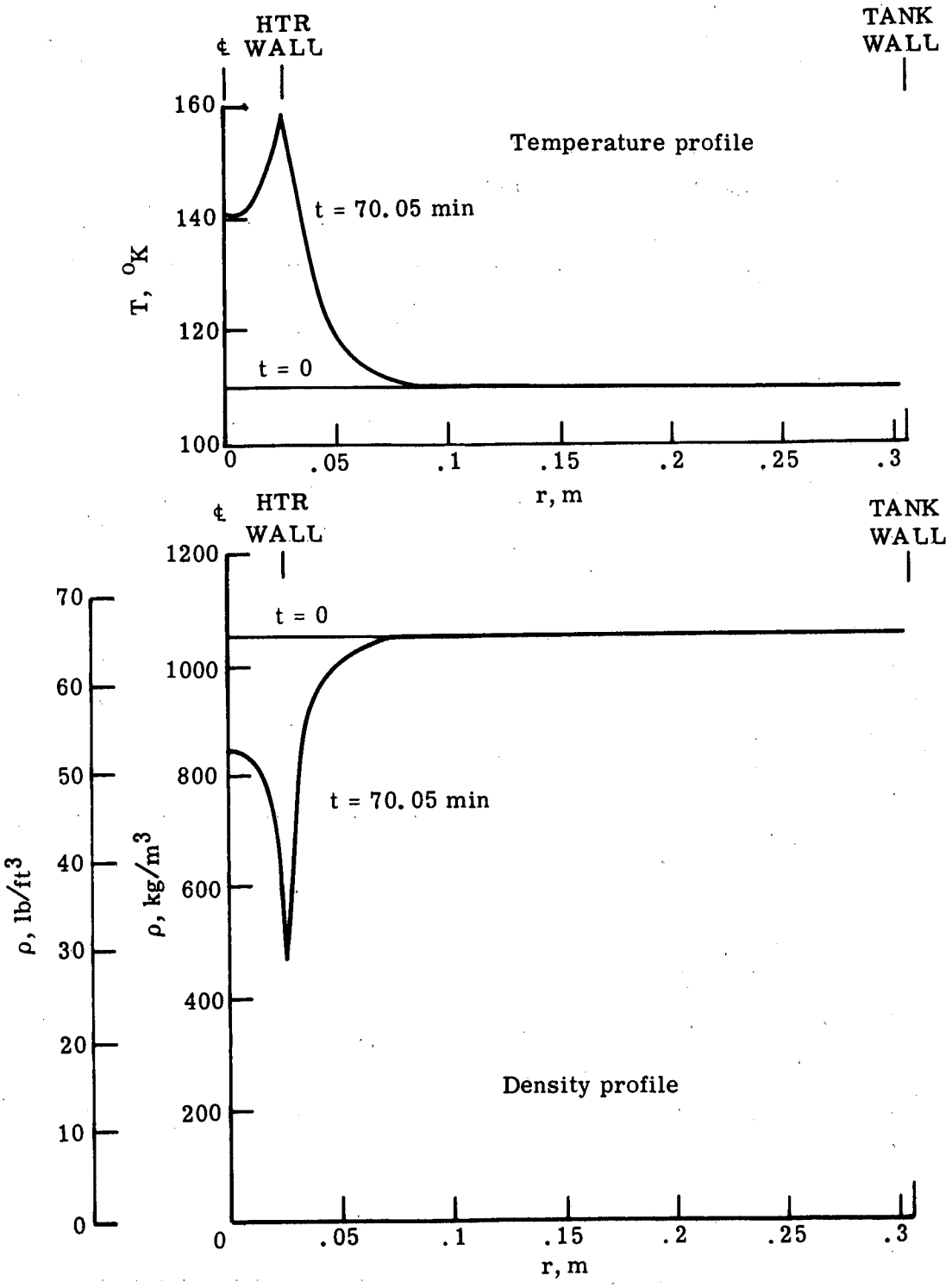

(a) Case 1.

Figure 5. - Profiles of temperature and density in tank for cases 1-4.

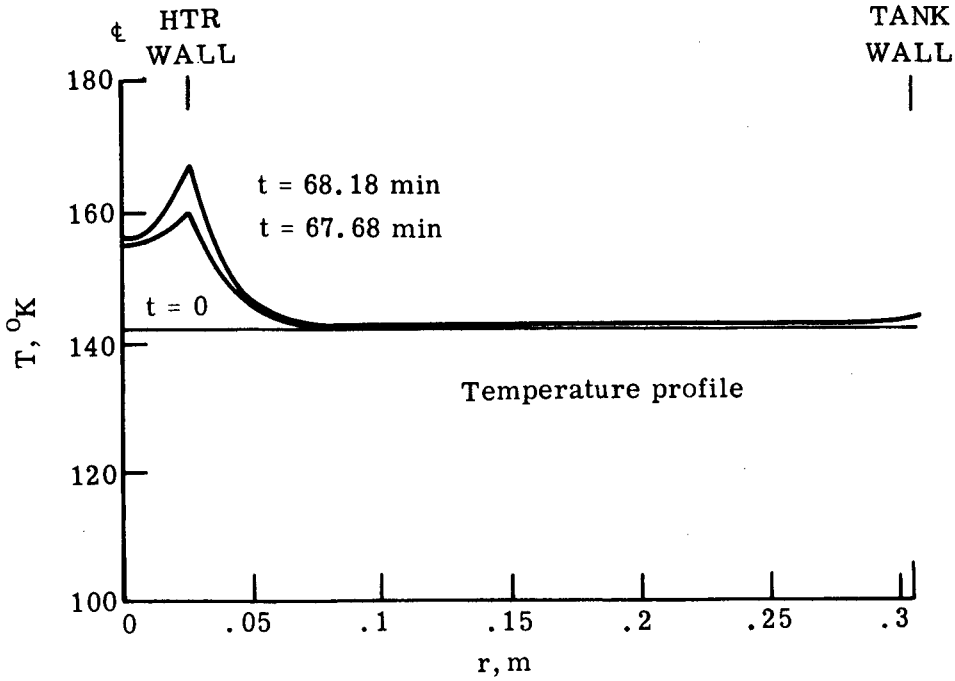

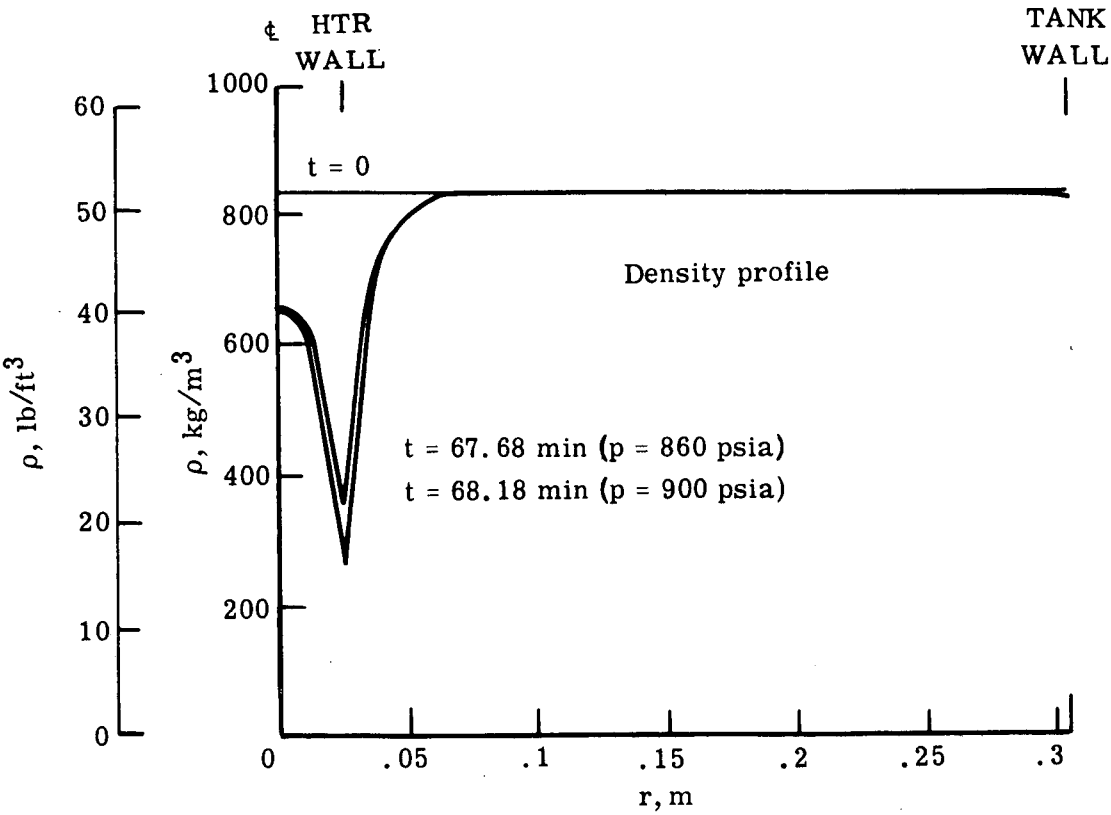

(b) Case 2.

Figure 5. - Continued.

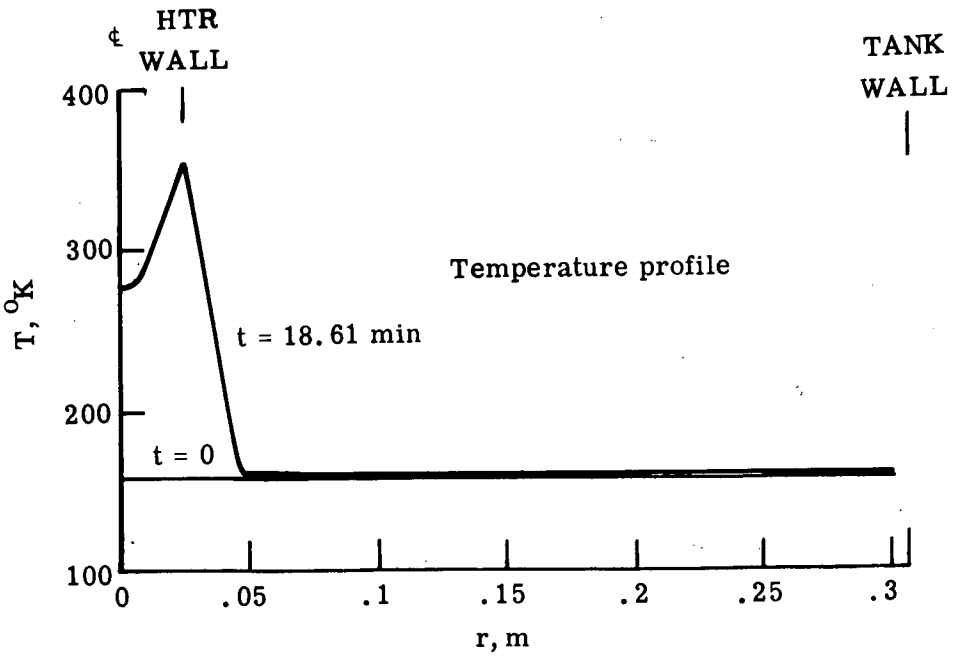

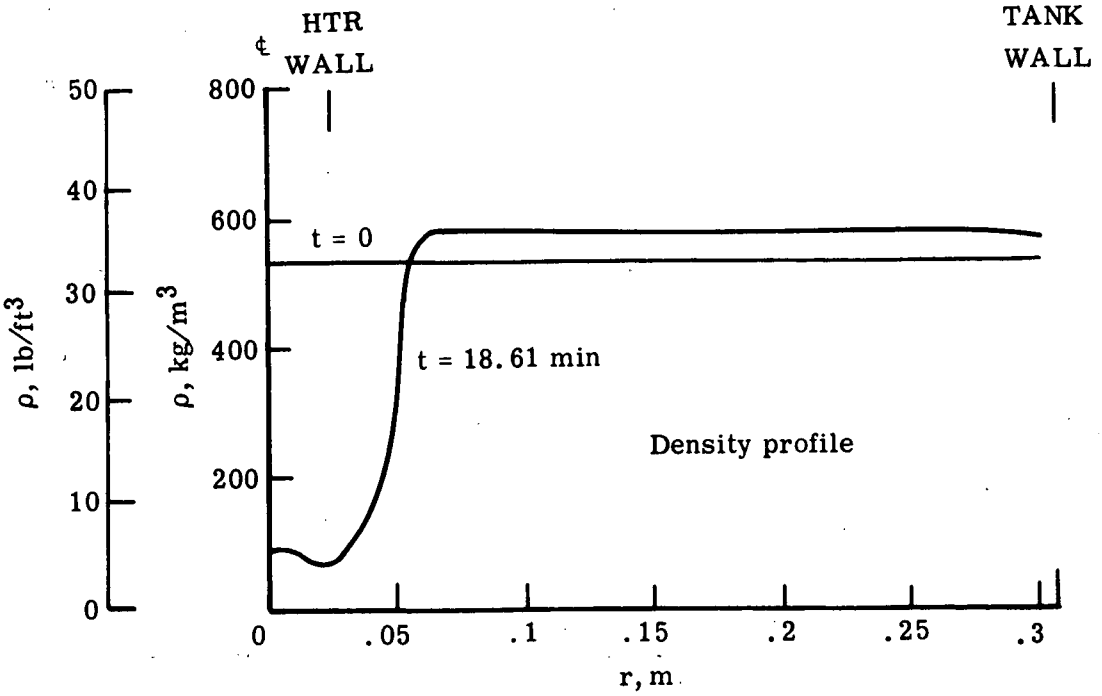

(c) Case 3.

Figure 5. - Continued.

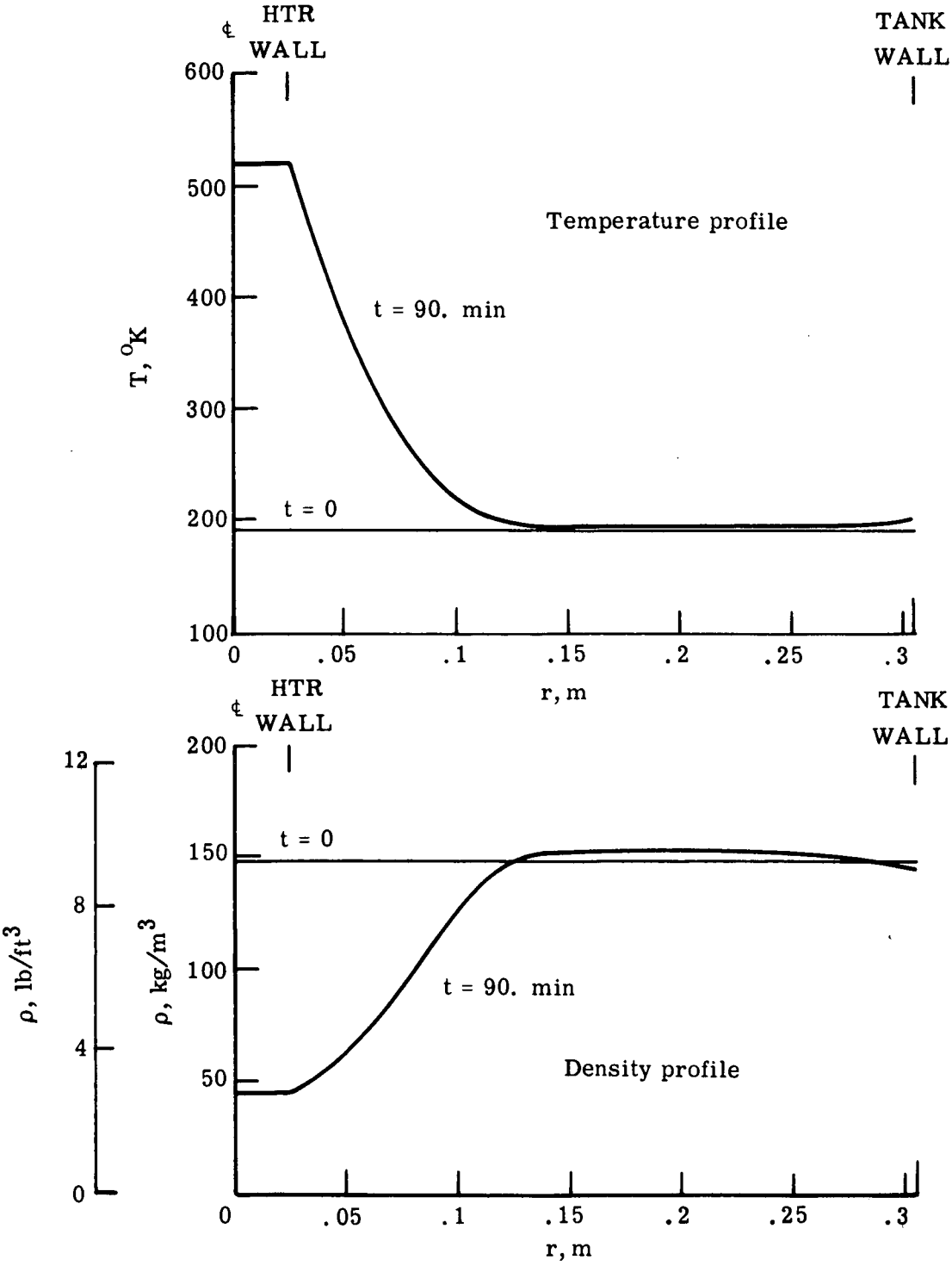

(d) Case 4.

Figure 5. - Concluded.

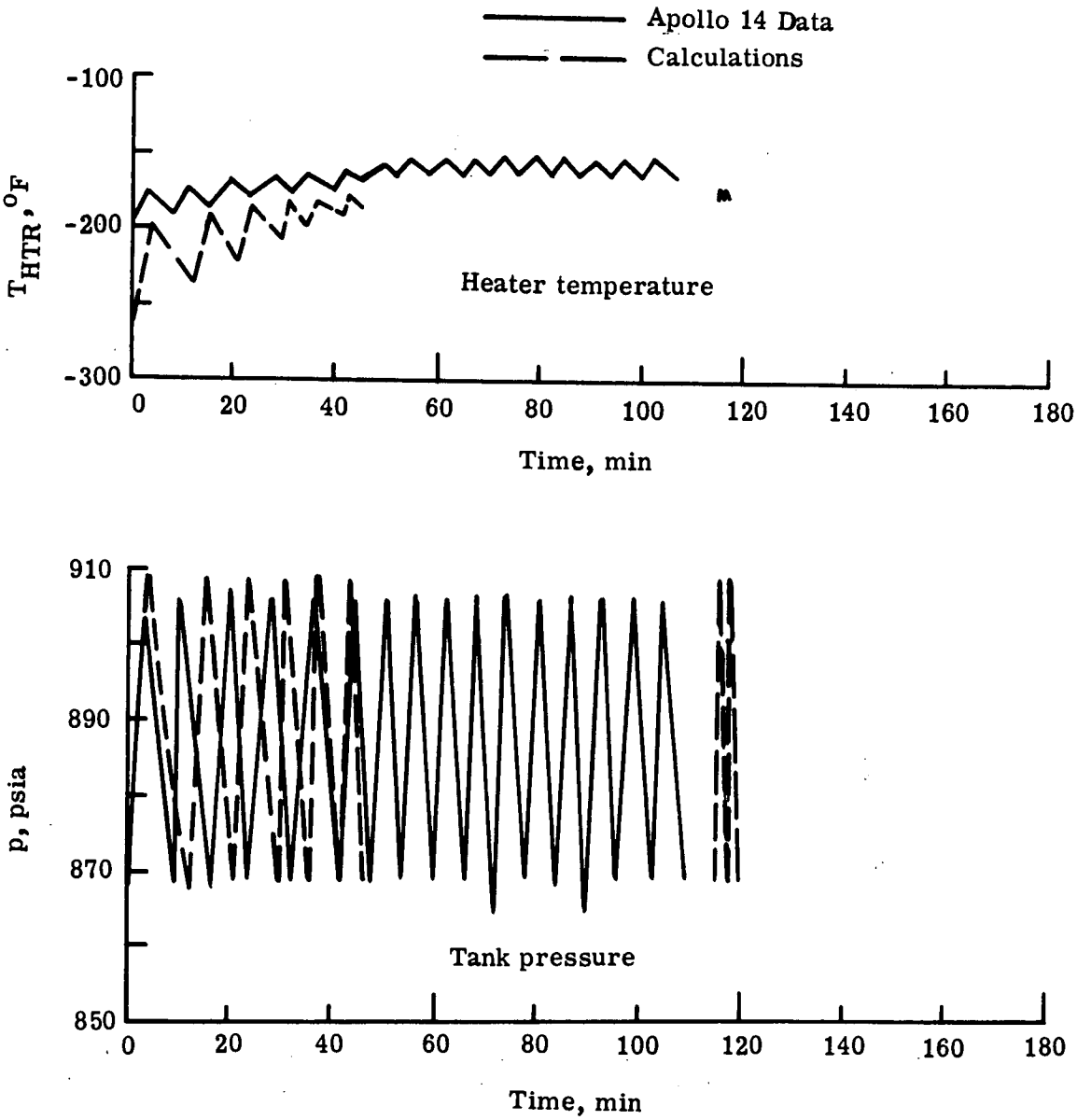

Figure 6.- Comparison of calculations for Case 1 with Apollo 14 flight data. Flight data begins at 10 hours 25 min. GET.

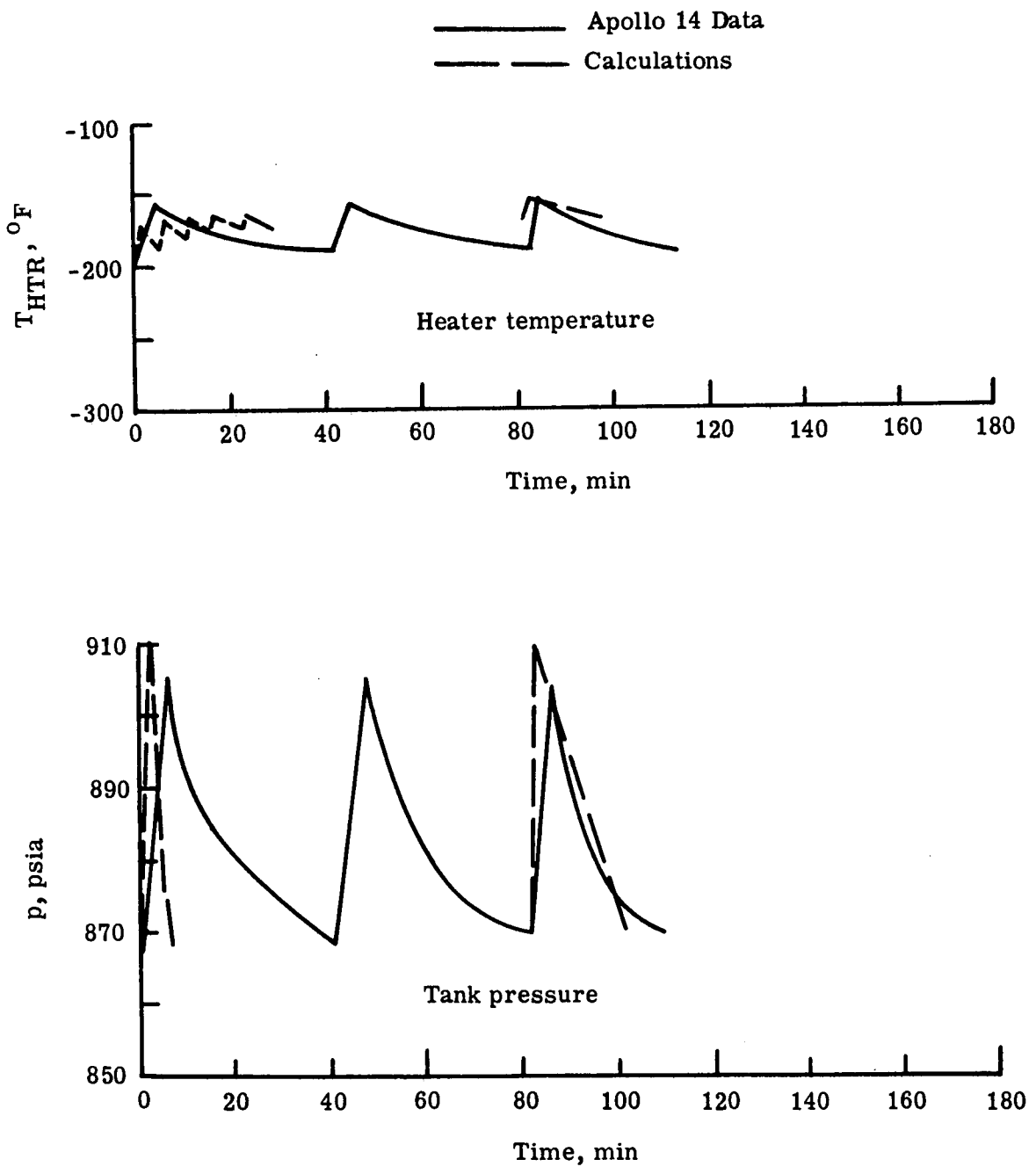

Figure 7.- Comparison of calculations for Case 2 with Apollo 14 flight data. Flight data begins at 151 hours GET.

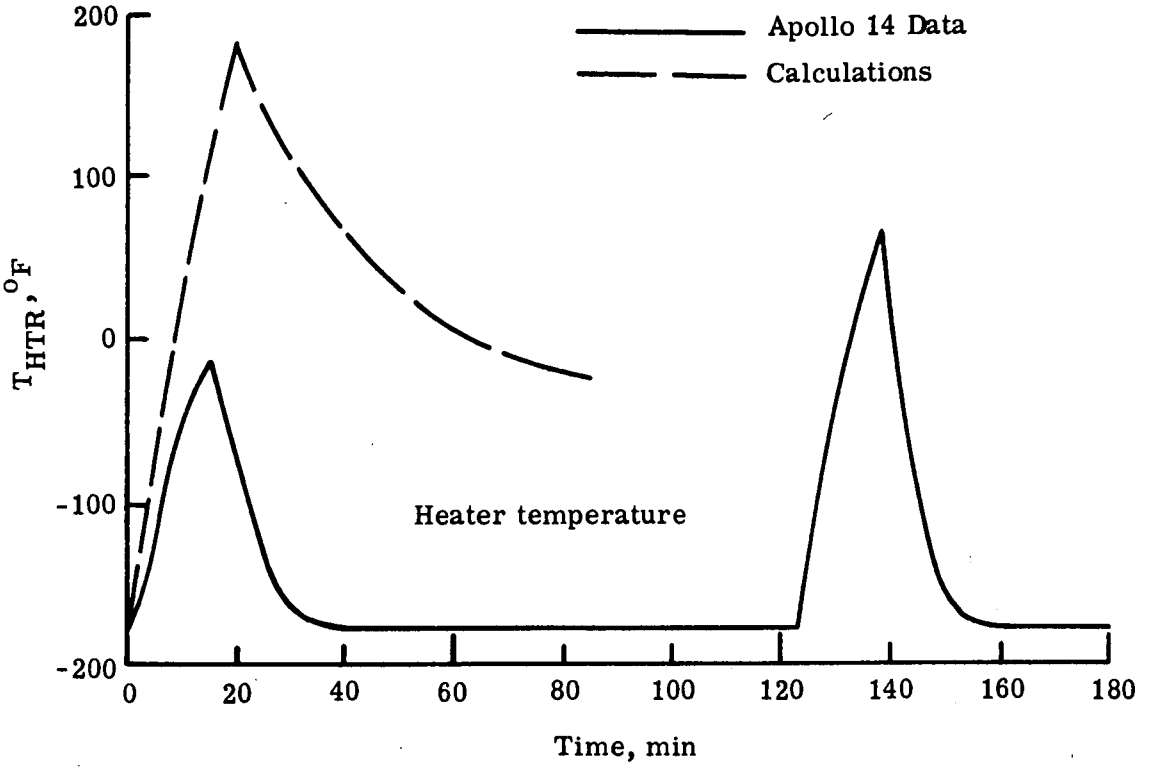

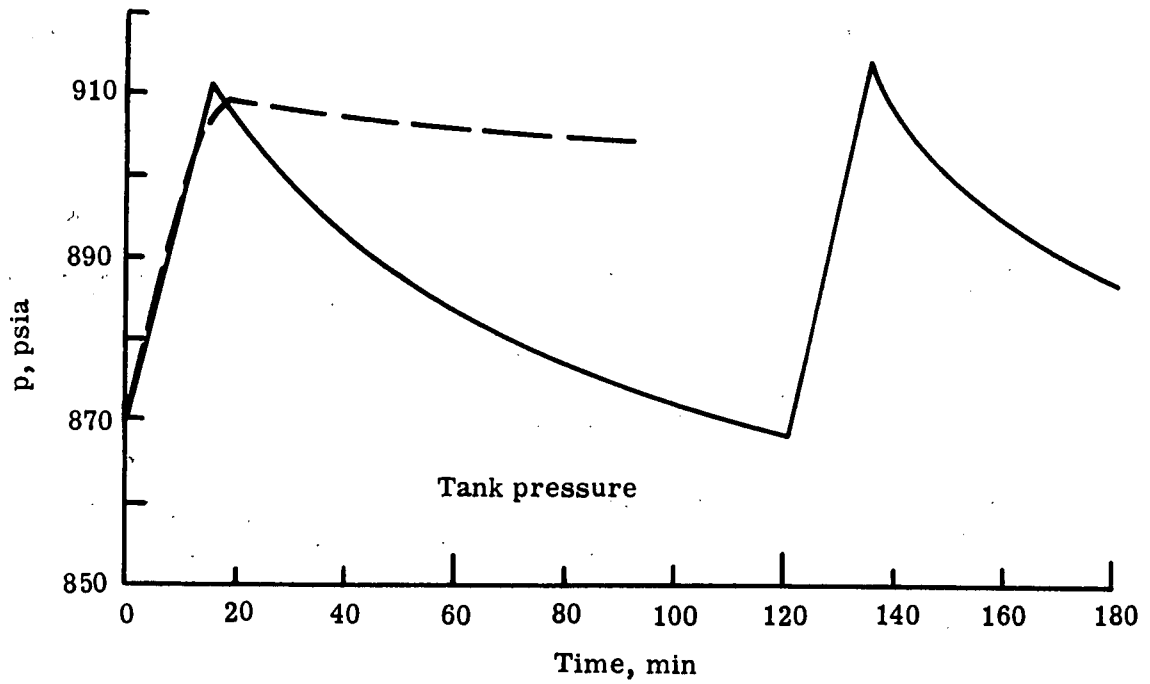

Figure 8.- Comparison of calculations for Case 3 with Apollo 14 flight data. Flight data begins at 30 hours 10 min. GET.

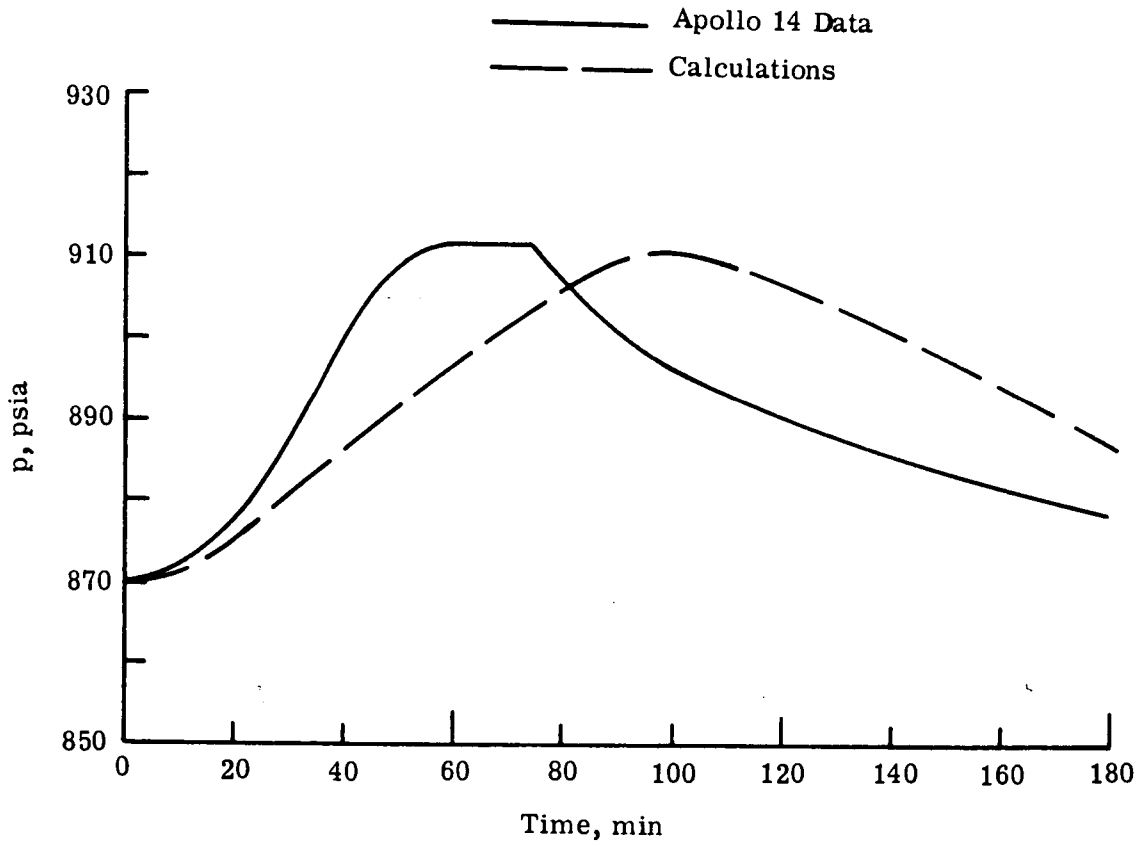

(a) Tank pressure.

Figure 9.- Comparison of calculations for Case 4 with Apollo 14 flight data. Flight data begins at 192 hours 20 min. GET.

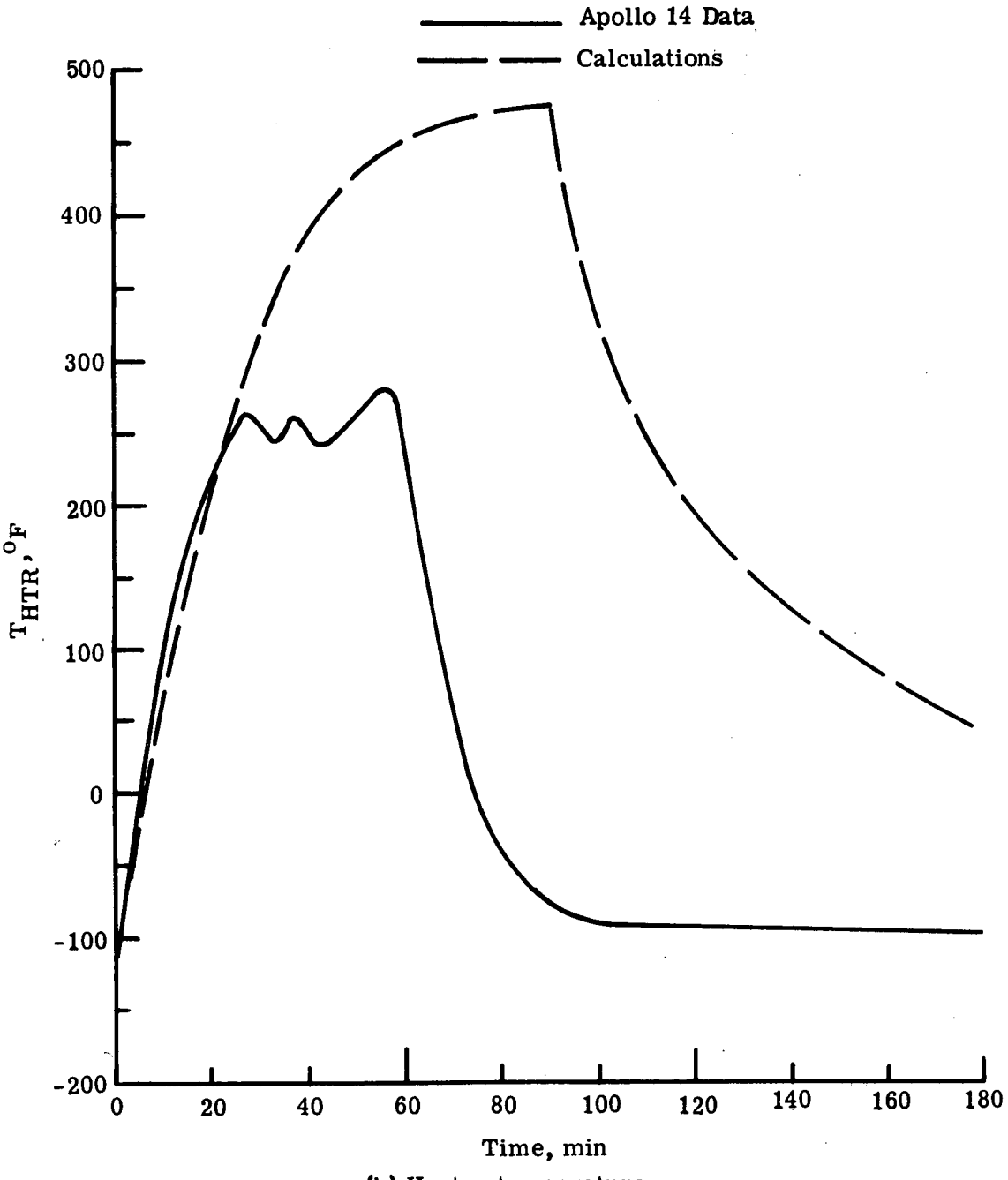

(b) Heater temperature.

Figure 9.- Concluded.